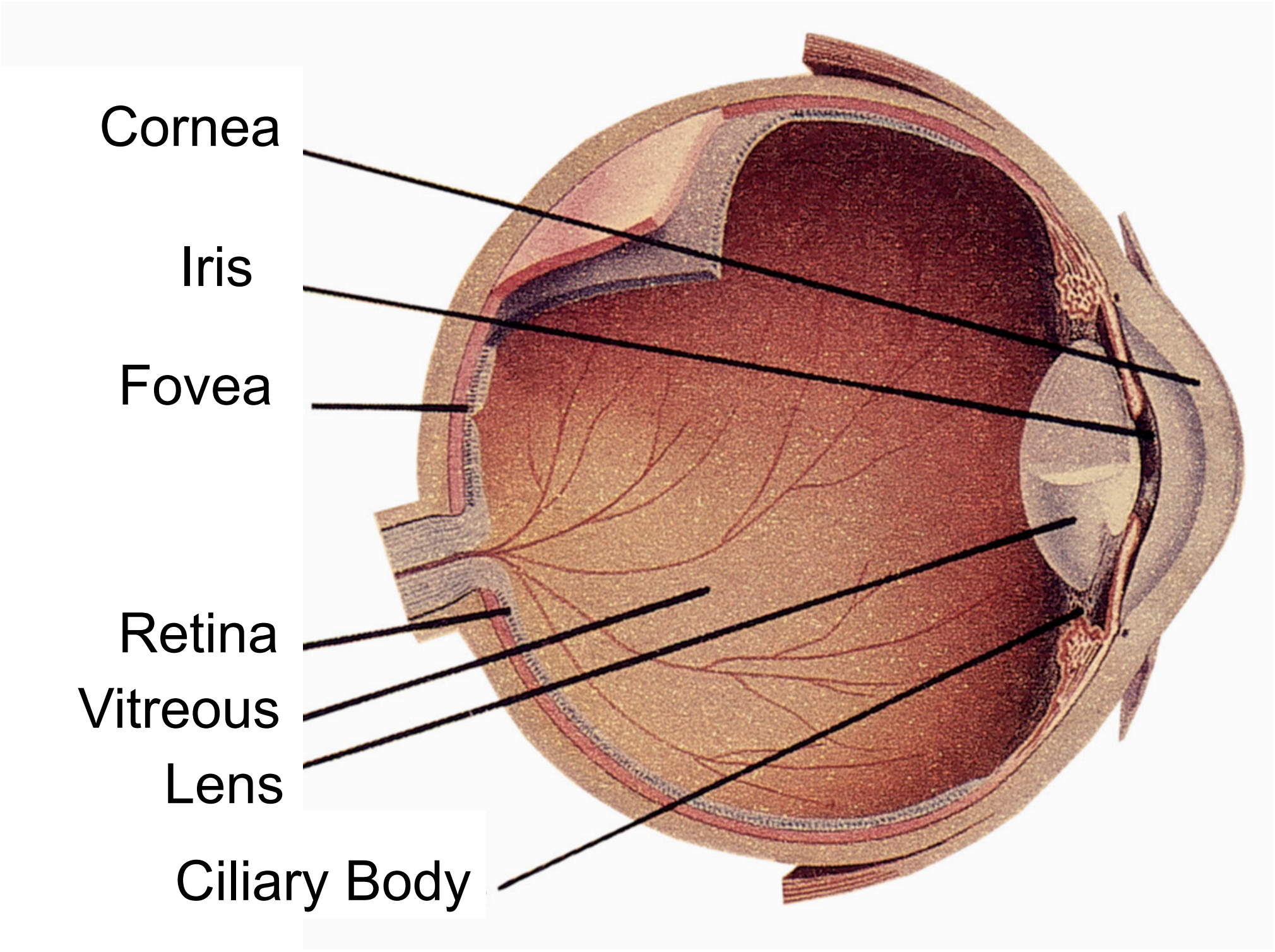
Cornea
Iris
Fovea
Retina
Vitreous
Lens
Ciliary Body

THE EXPERIMENT OF HECHT, SCHLAER, AND PIRENNE

IN 1942, Hecht, Schlaer, and Pirenne reported an experiment of extraordinary significance.[1] They presented flashes of light to normal human subjects, and determined the lowest possible intensity of that light that the subjects could see. The results were extremely surprising, and led immediately to many strong conclusions about the structure of the visual system and the nature of perceptual processes.

Their experiment is also very useful in a different way. The considerations that Hecht *et al.* had to entertain in order to design and perform the experiment form a useful outline of a large part of our knowledge of perceptual phenomena and of their underlying physiological processes. These considerations, and the results of the experiment, will be described briefly in this chapter and elaborated in succeeding chapters.

General design
Dark adaptation
Location of the test flash
Size of the test flash
Duration of the test flash
Color of the test flash
Interpretation

ENERGY, QUANTA, AND VISION*

By SELIG HECHT, SIMON SHLAER, and MAURICE HENRI PIRENNE‡

(*From the Laboratory of Biophysics, Columbia University, New York*)

(Received for publication, March 30, 1942)

I

Threshold Energies for Vision

The minimum energy required to produce a visual effect achieves its significance by virtue of the quantum nature of light. Like all radiation, light is emitted and absorbed in discrete units or quanta, whose energy content is equal to its frequency ν multiplied by Planck's constant h. At the threshold of vision these quanta are used for the photodecomposition of visual purple, and in conformity with Einstein's equivalence law each absorbed quantum transforms one molecule of visual purple (Dartnall, Goodeve, and Lythgoe, 1938). Since even the earliest measurements show that only a small number of quanta is required for a threshold stimulus, it follows that only a small number of primary molecular transformations is enough to supply the initial impetus for a visual act. The precise number of these molecular changes becomes of obvious importance in understanding the visual receptor process, and it is this which has led us to the present investigation.

after Cornsweet, 1970

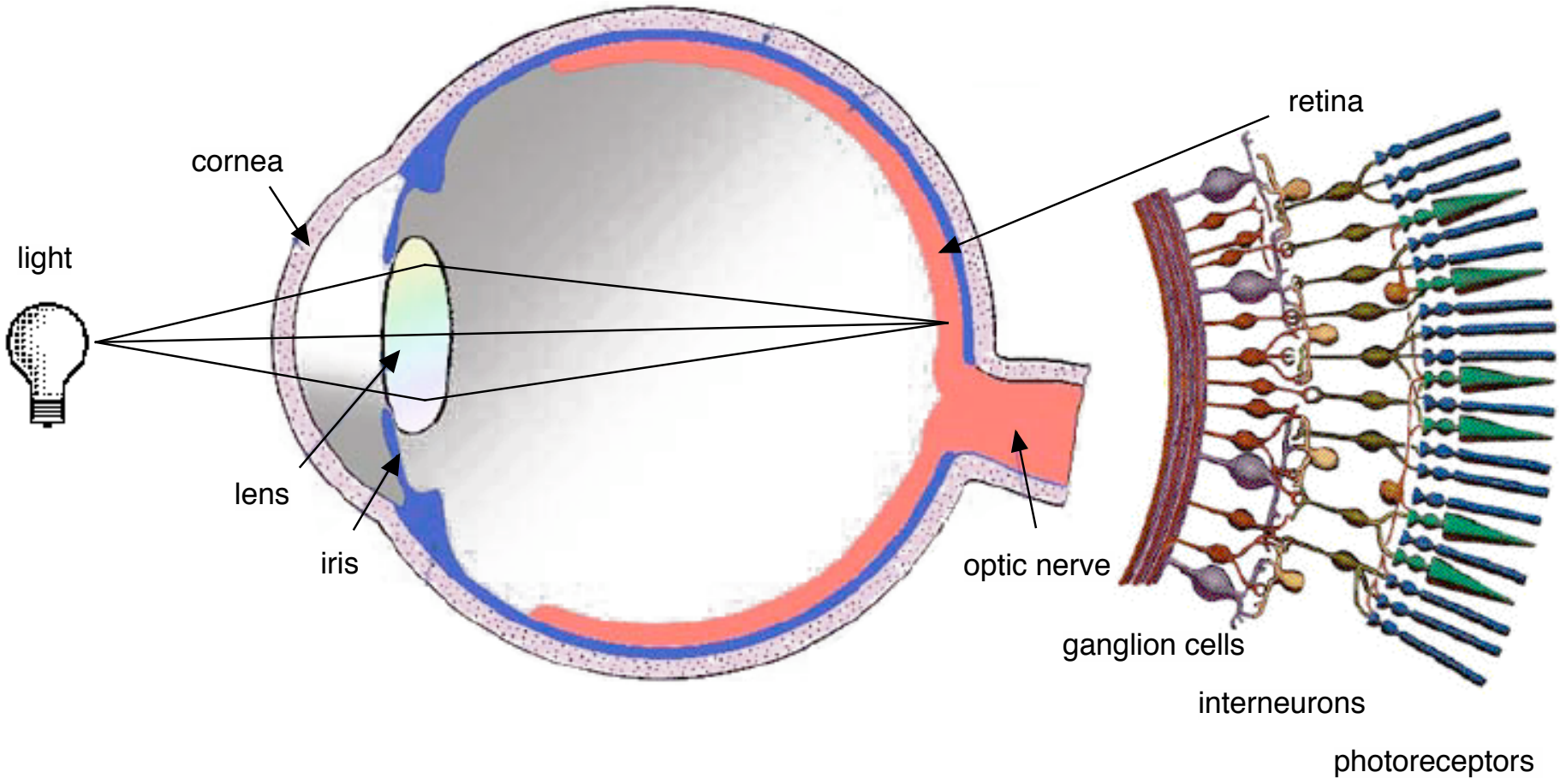
retina
cornea
light
lens
iris
optic nerve
ganglion cells
interneurons
photoreceptors

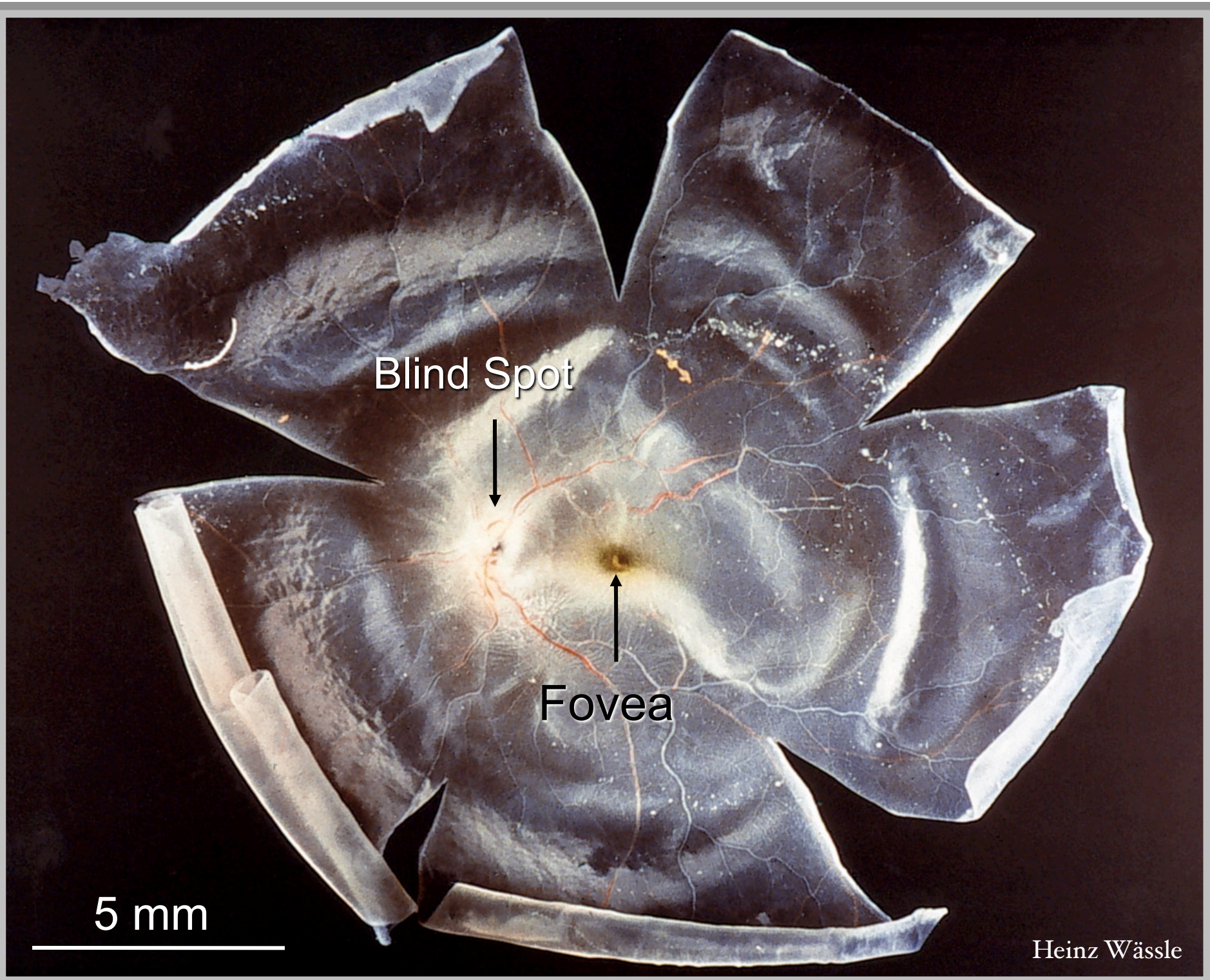
Blind Spot
Fovea
5 mm
Heinz Wässle

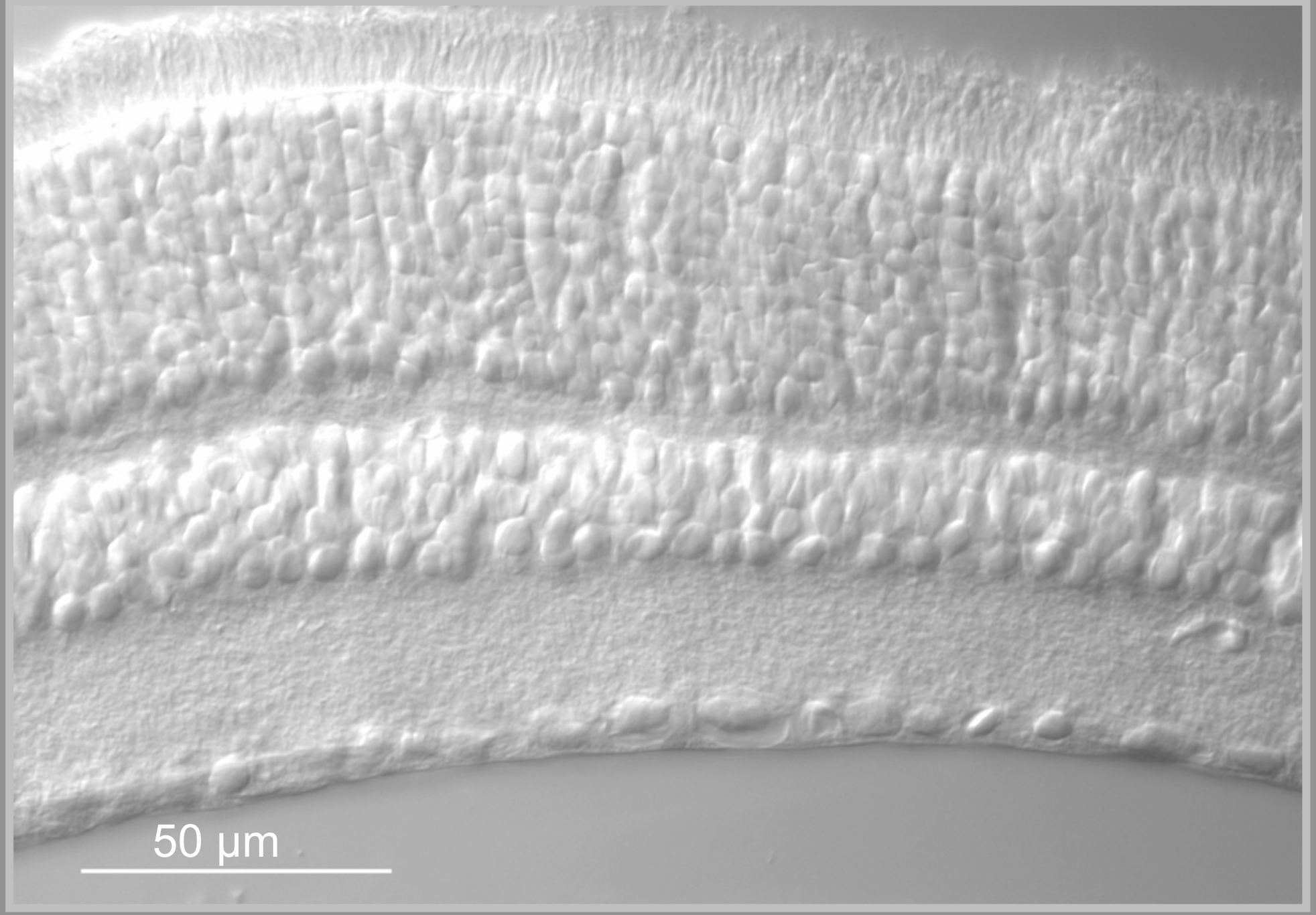

Heinz Wässle

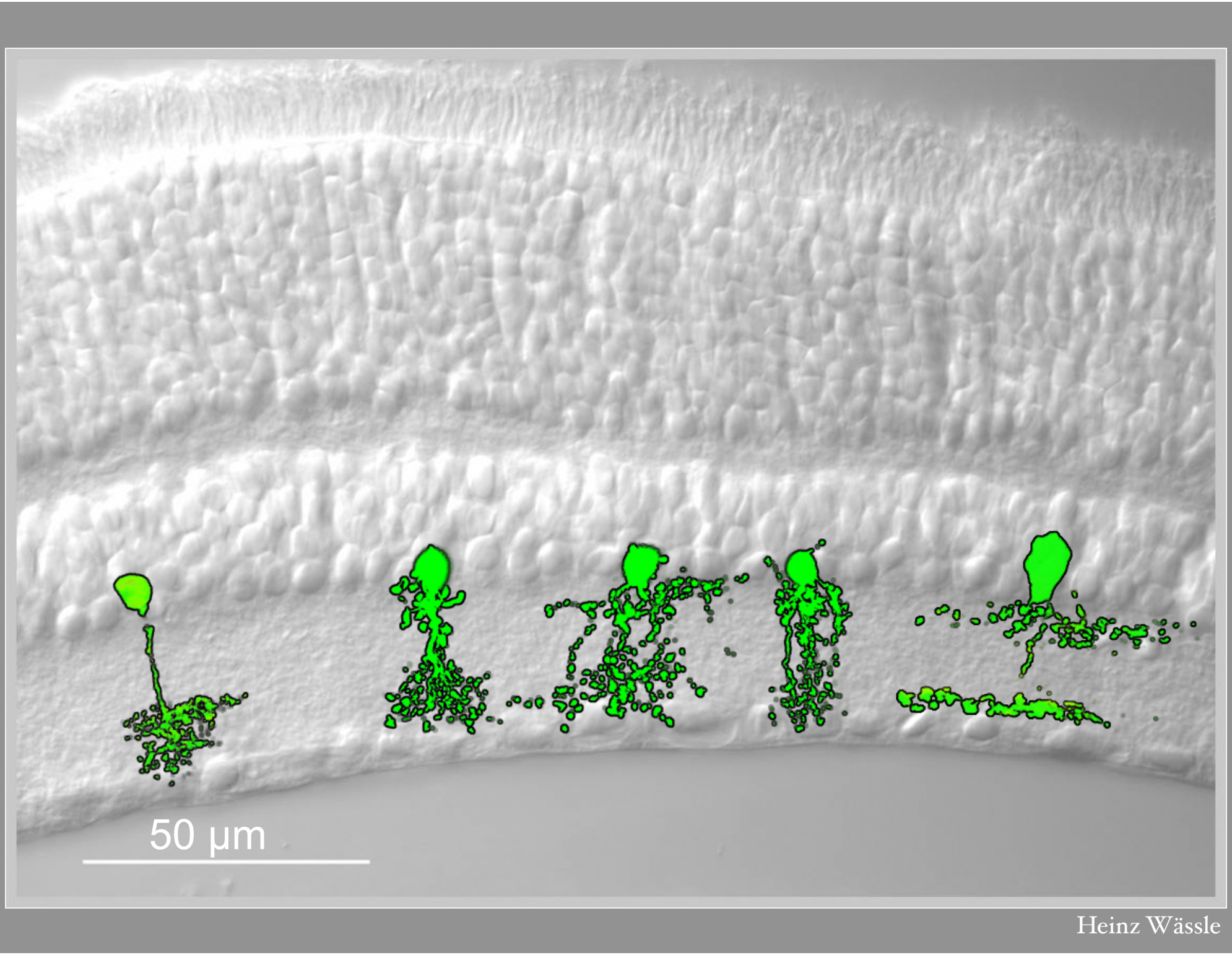

Heinz Wässle

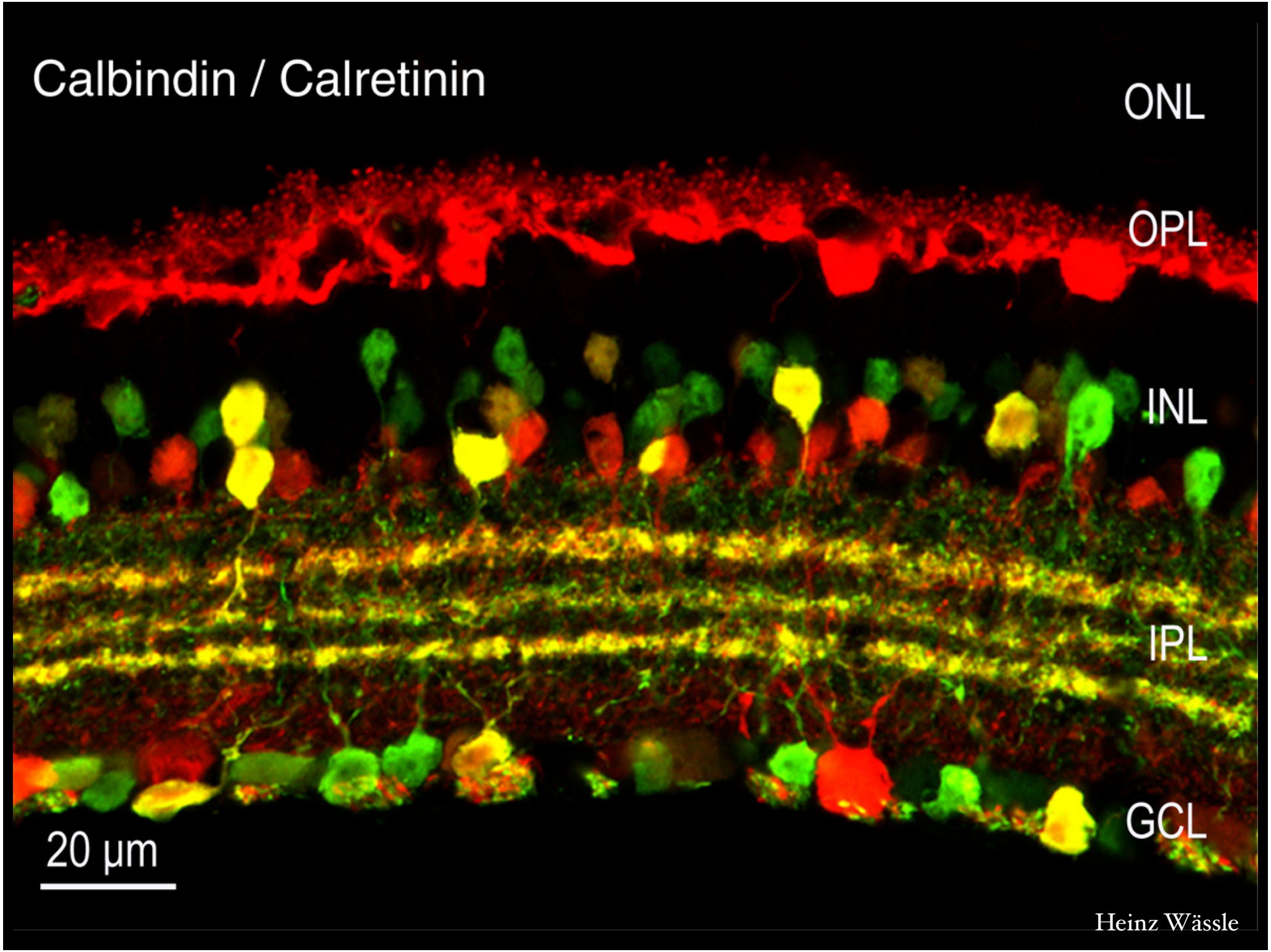
Calbindin / Calretinin
ONL
OPL
INL
IPL
GCL
20 µm
Heinz Wässle

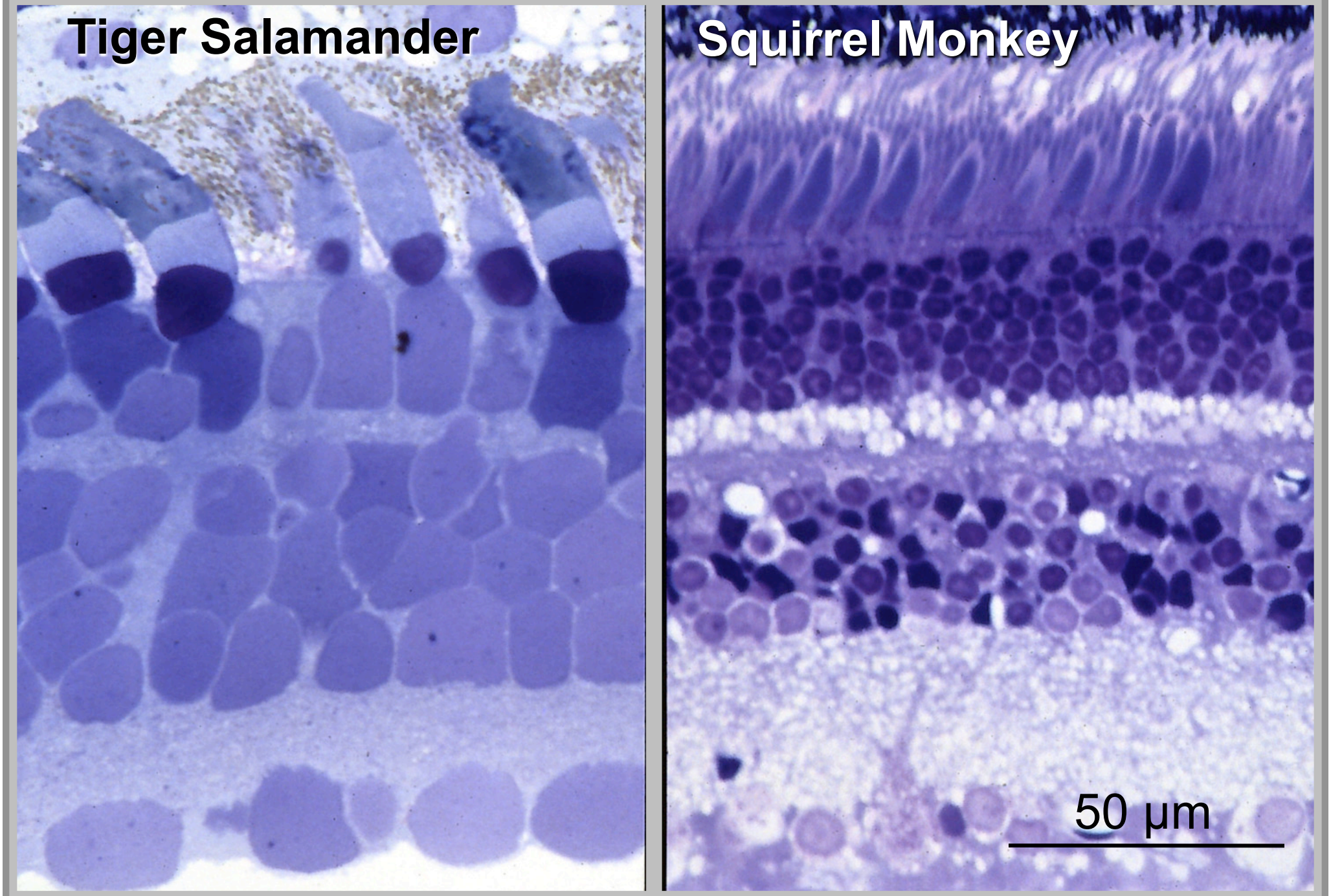
Tiger Salamander
Squirrel Monkey
50 µm

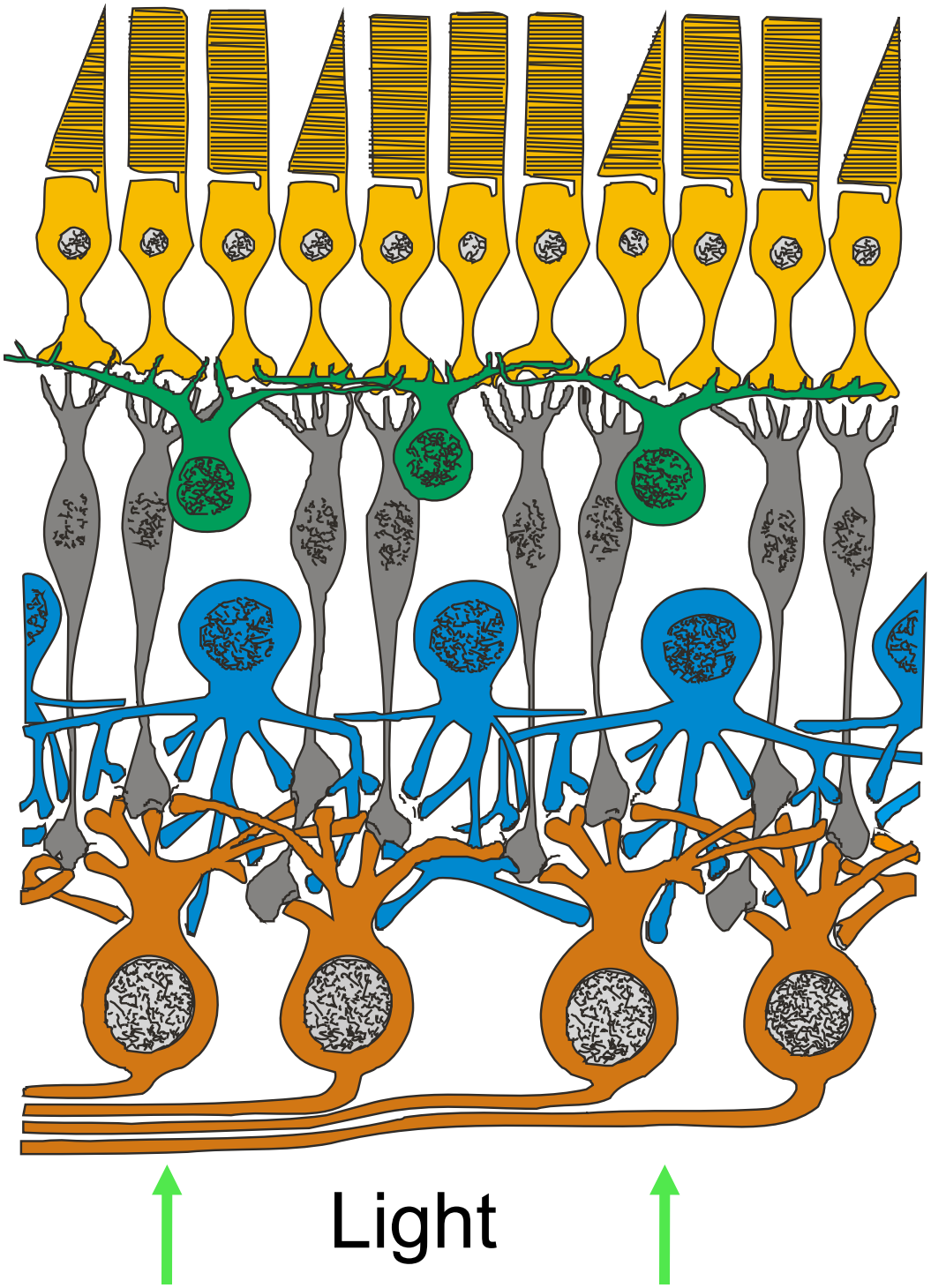

Photoreceptors

Horizontal Cells

Bipolar Cells

Amacrine Cells

Ganglion Cells

Heinz Wässle

Vertical and horizontal pathways for information flow in the retina

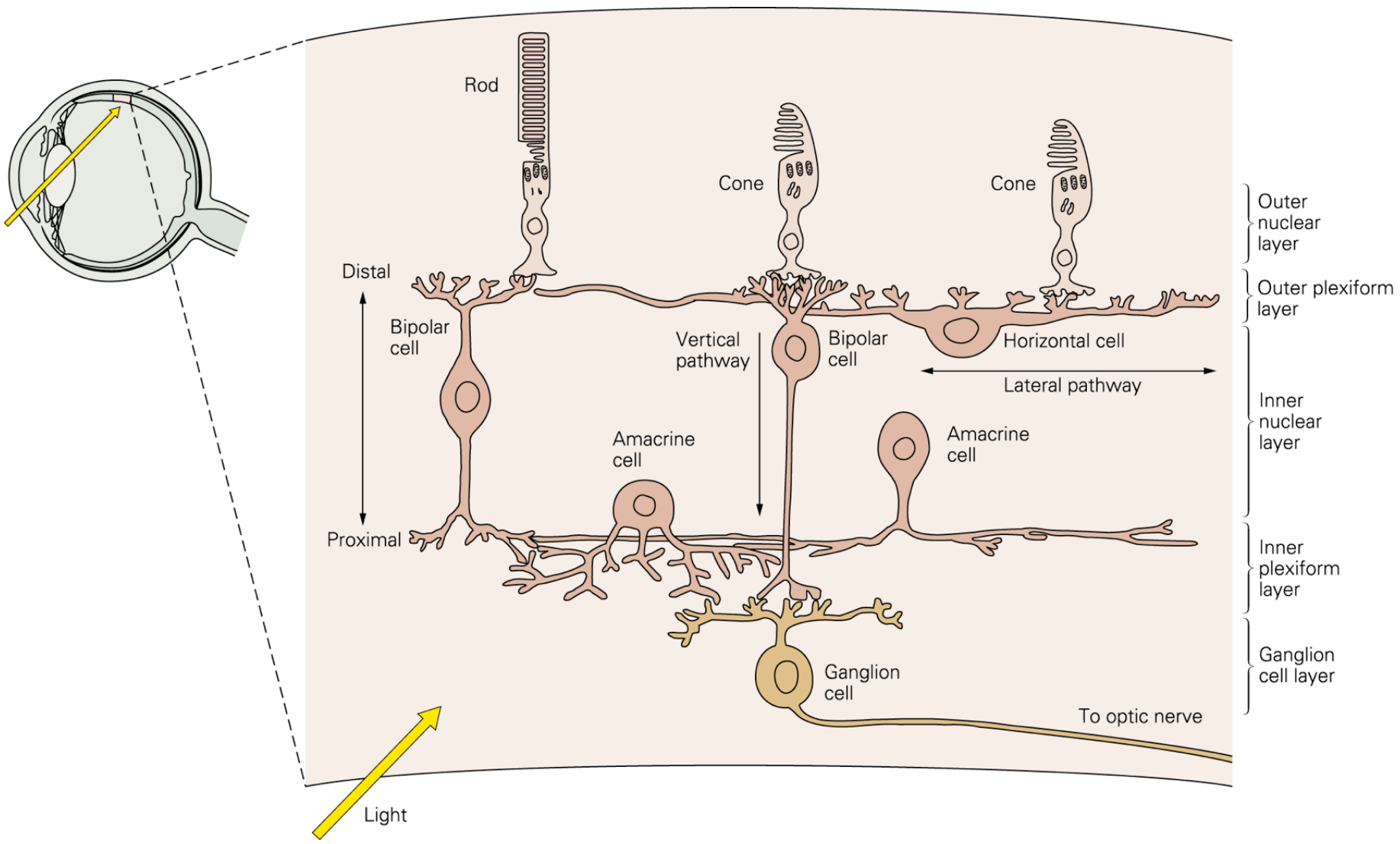

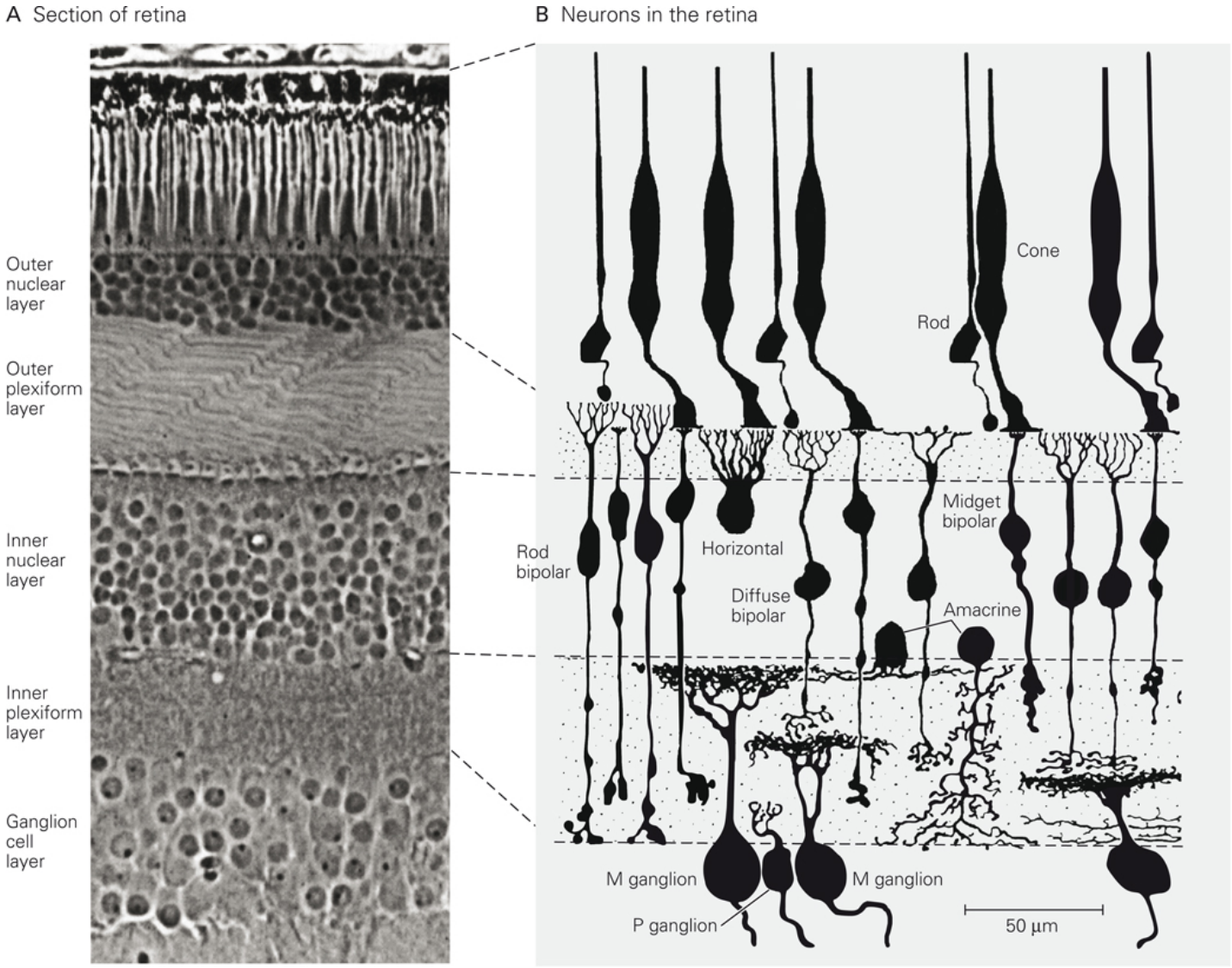

Figure 26–2 The retina comprises five distinct layers of neurons and synapses.

A. A perpendicular section of the human retina seen through the light microscope. Three layers of cell bodies are evident. The outer nuclear layer contains cell bodies of photoreceptors; the inner nuclear layer includes horizontal, bipolar, and amacrine cells; and the ganglion cell layer contains ganglion cells and some displaced amacrine cells. Two layers of fibers and synapses separate these: the outer plexiform layer and the inner plexiform layer. (Reproduced, with permission, from Boycott and Dowling 1969.)

B. Neurons in the retina of the macaque monkey based on Golgi staining. The cellular and synaptic layers are aligned with the image in part A. (**M ganglion**, magnocellular ganglion cell; **P ganglion**, parvocellular ganglion cell.) (Reproduced, with permission, from Polyak 1941.)

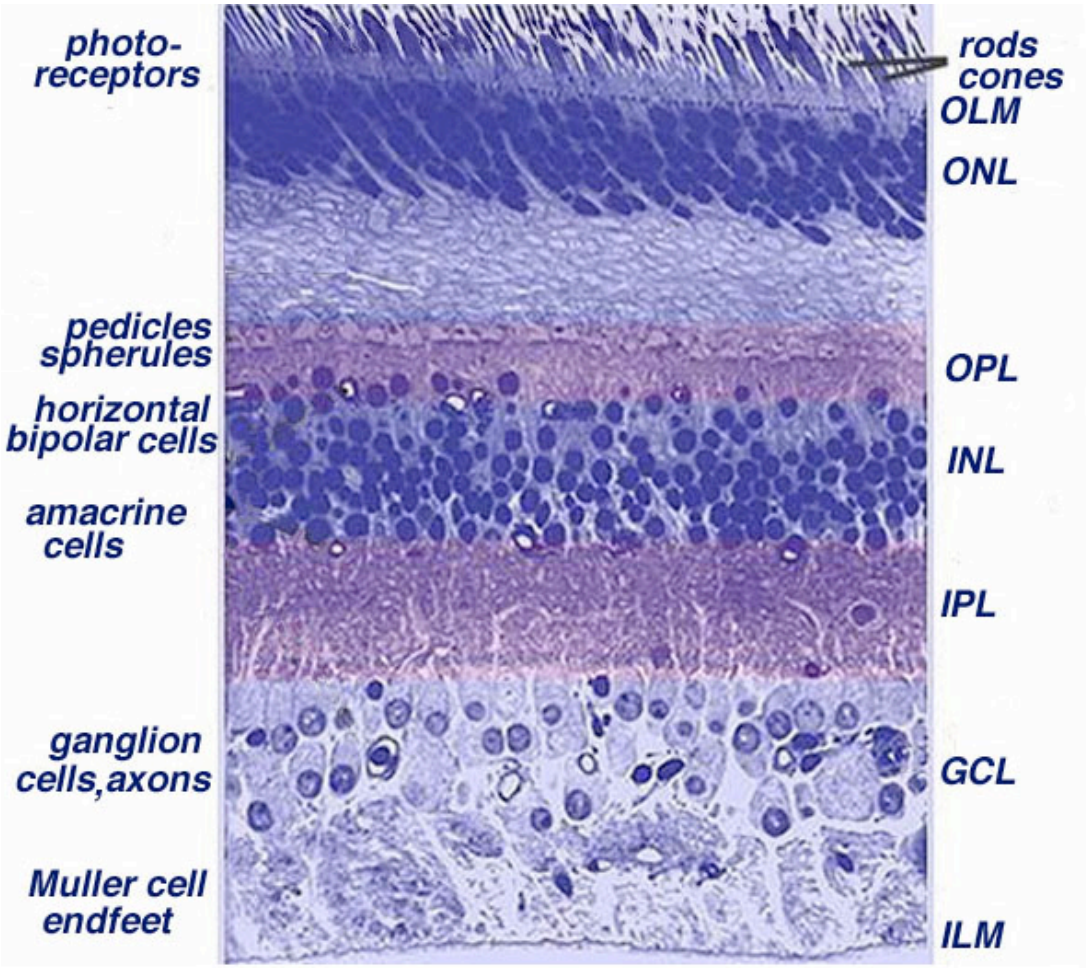

Fig. 3. Light micrograph of a vertical section through central human retina.

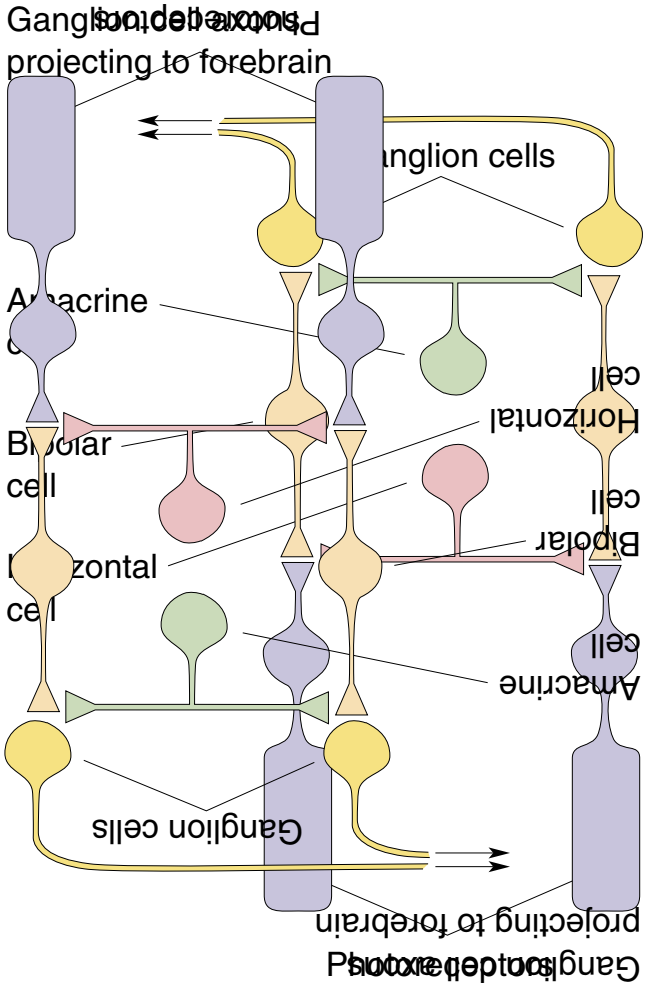

The distribution of rods and cones in human retina

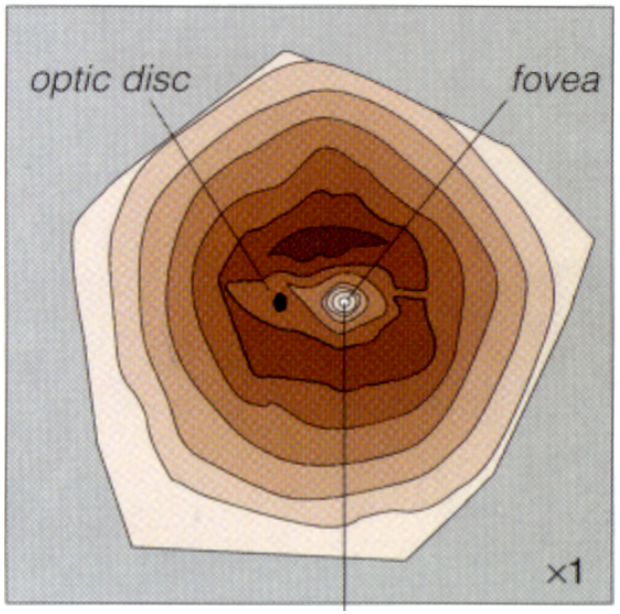

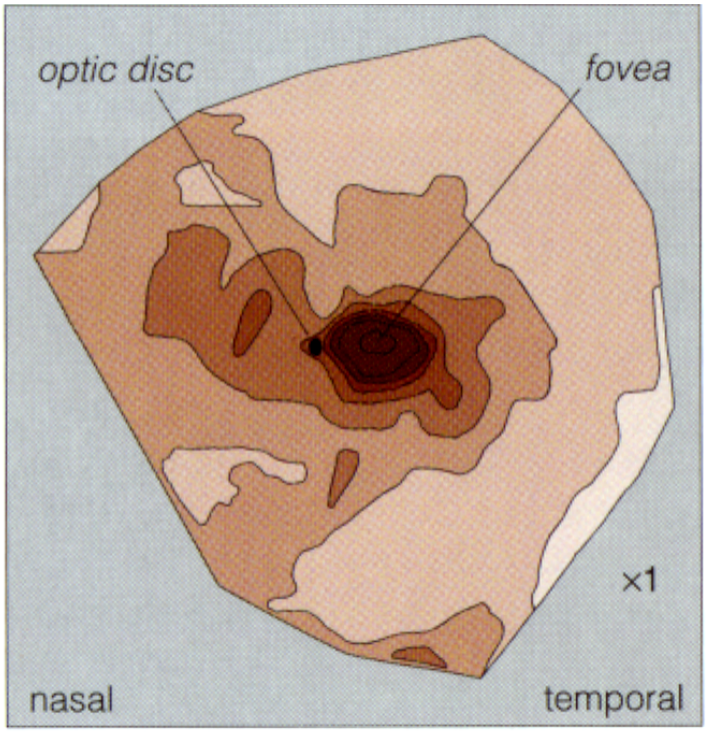

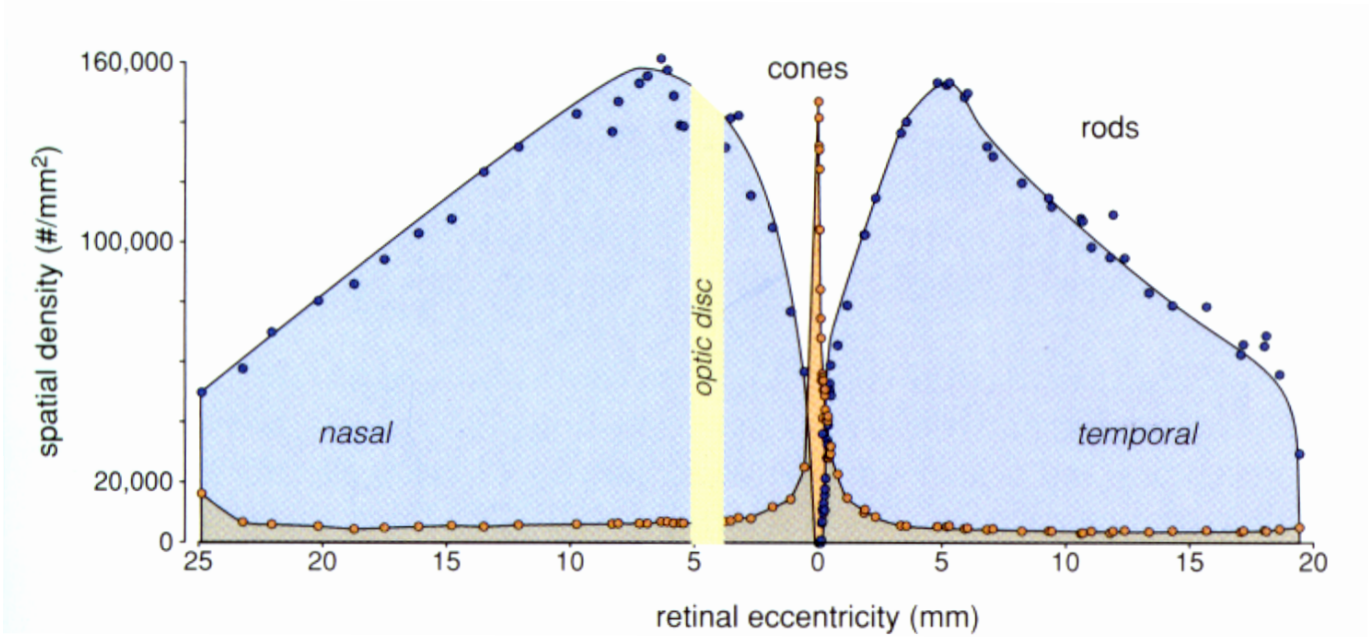

The distribution of rods and cones in human retina

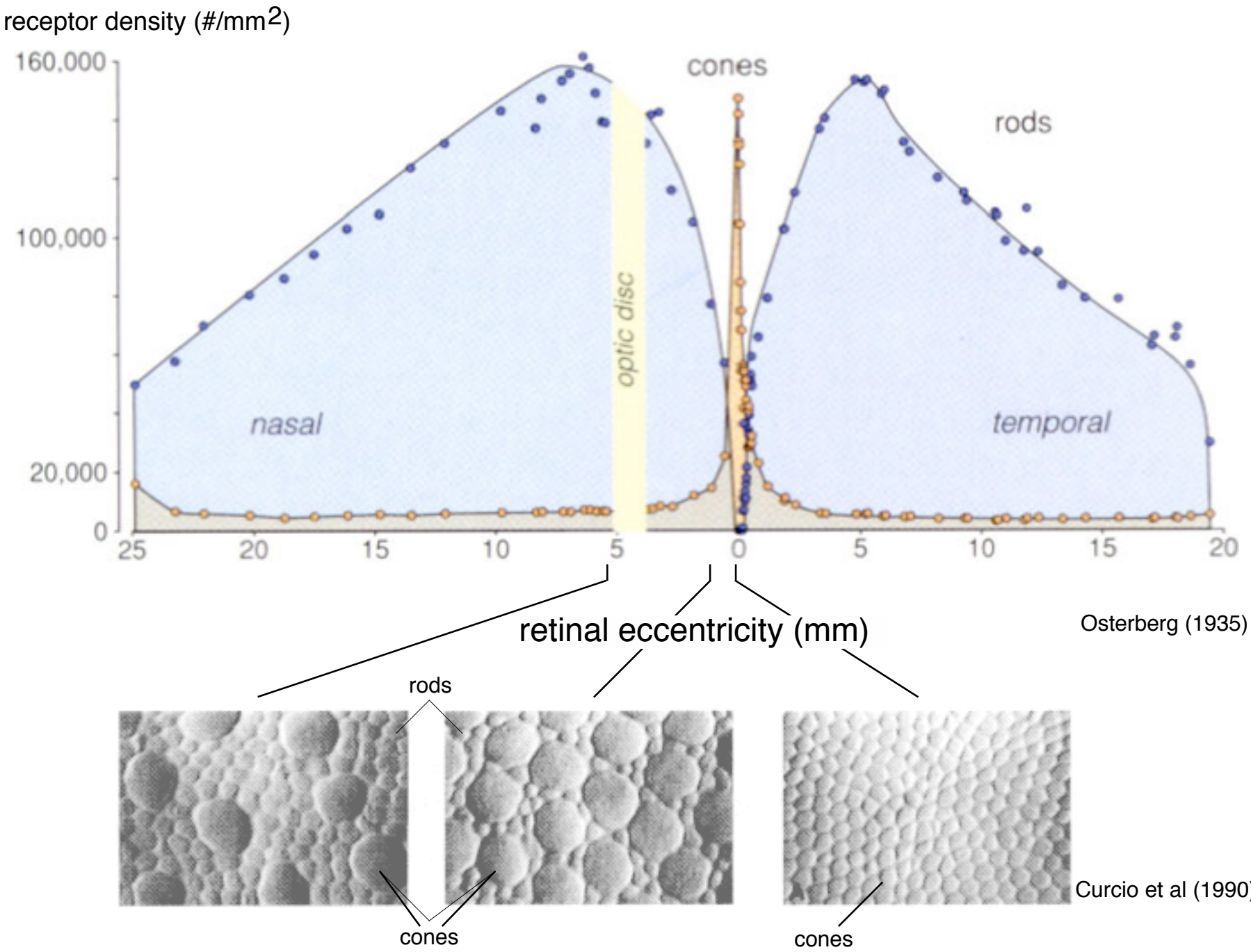

Osterberg (1935)

Curcio et al (1990)

The parafovea

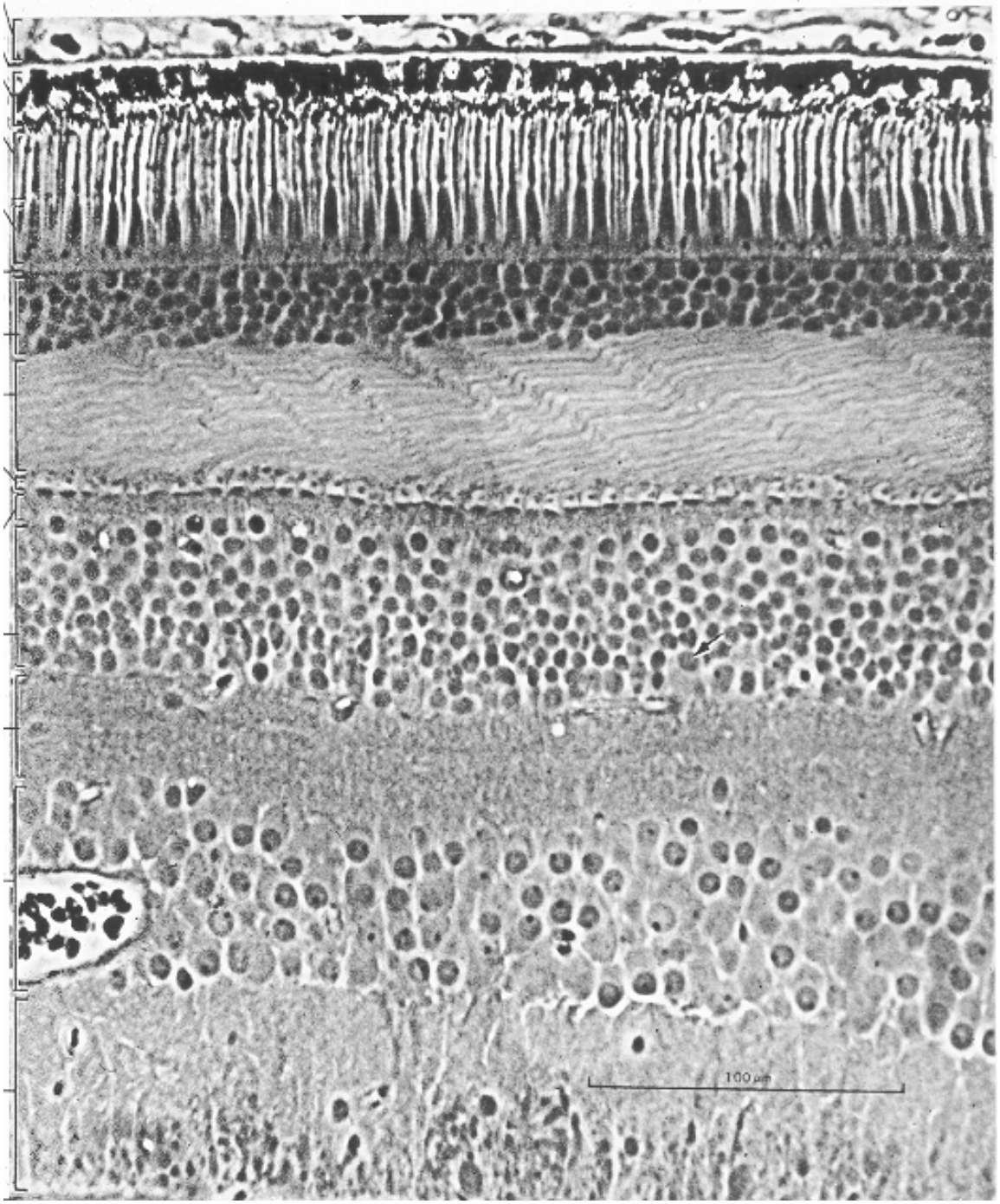

The foveal slope

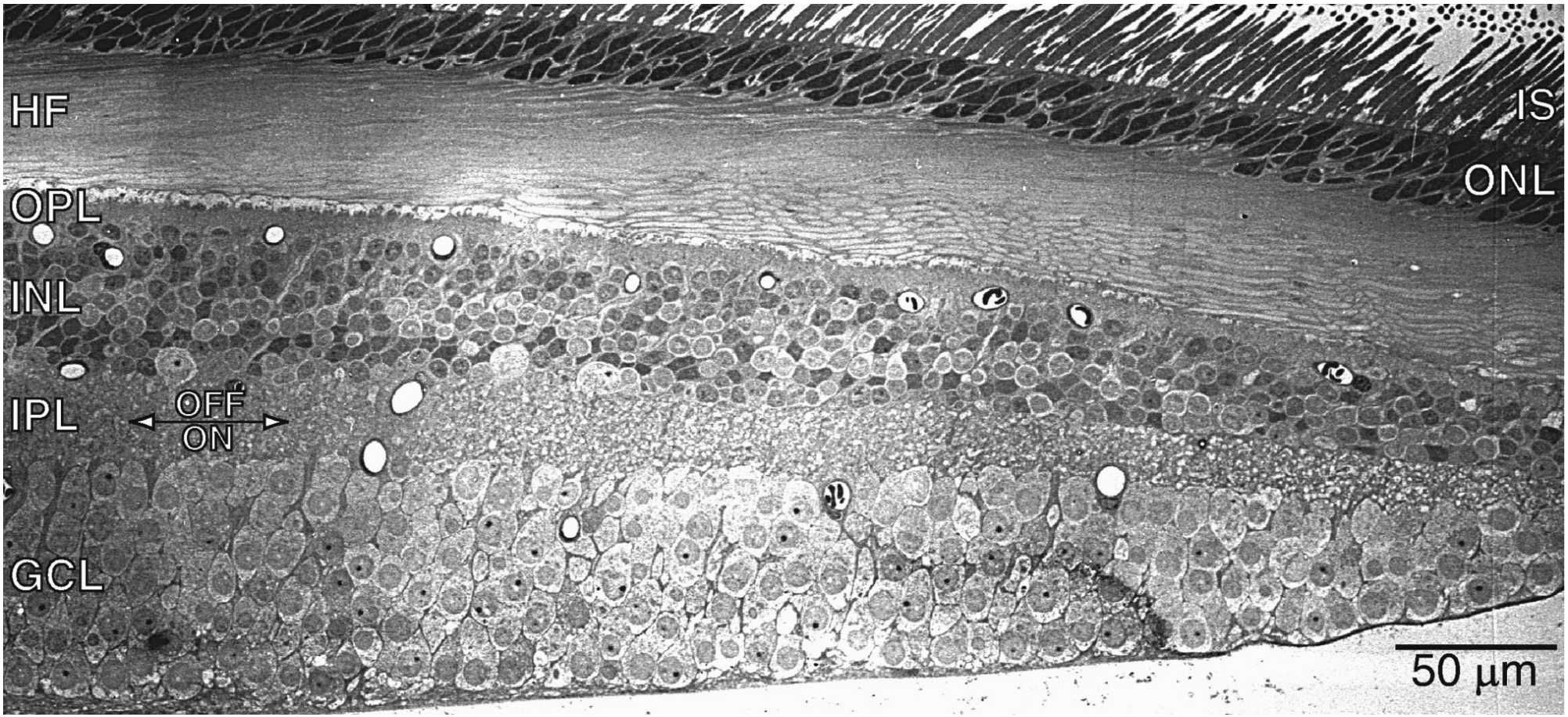

The fovea

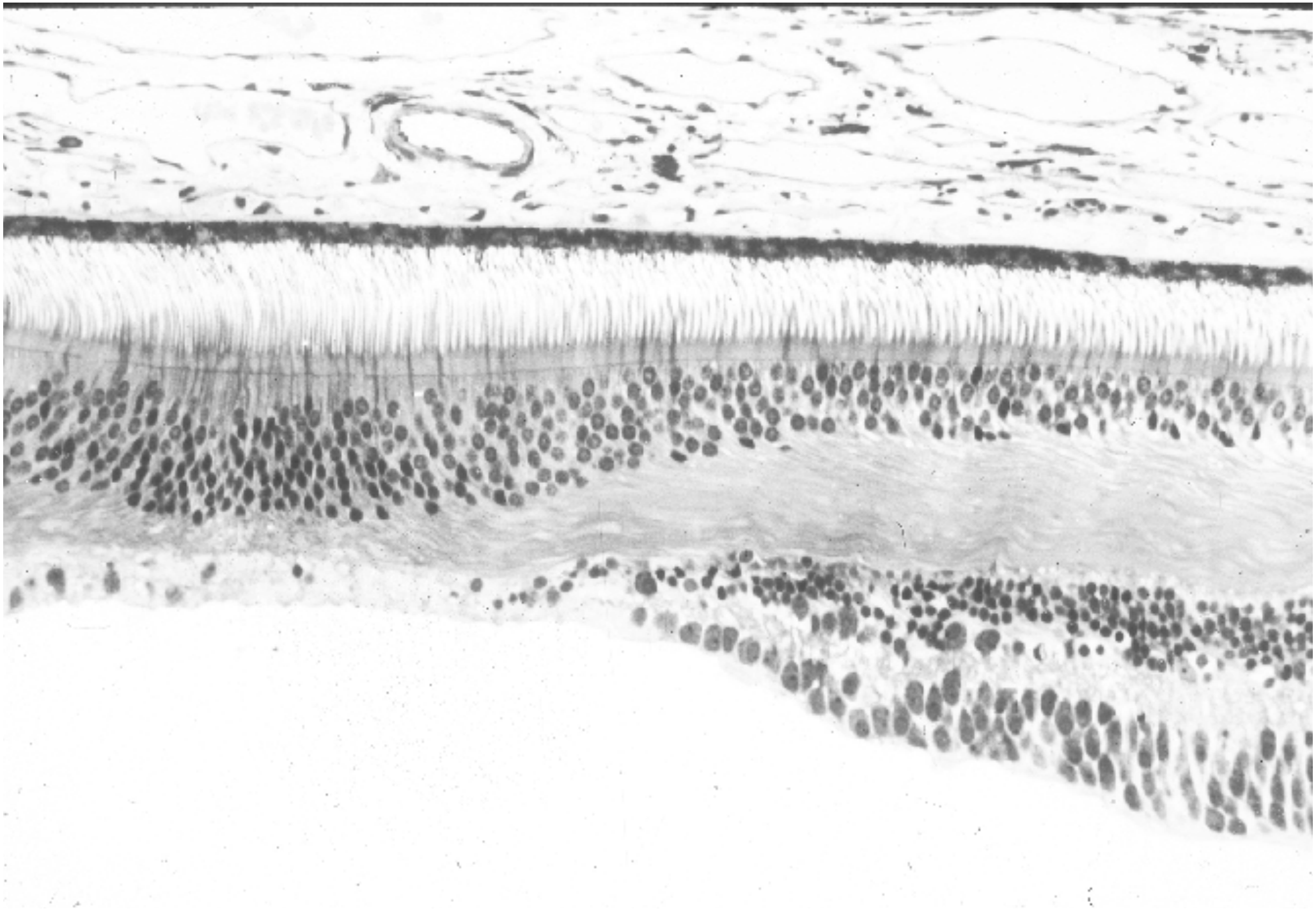

The foveal cone mosaic

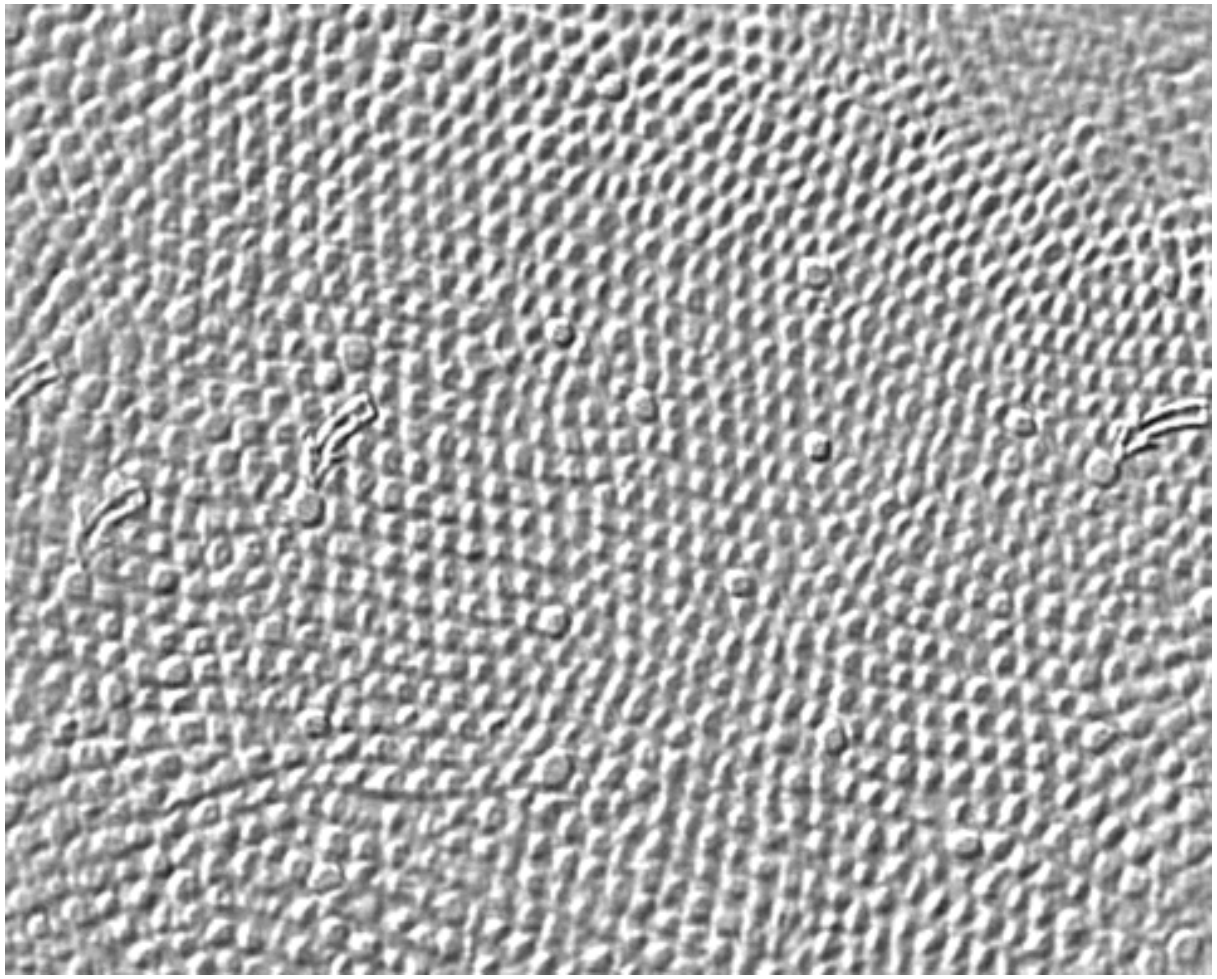

Polyak (1941)

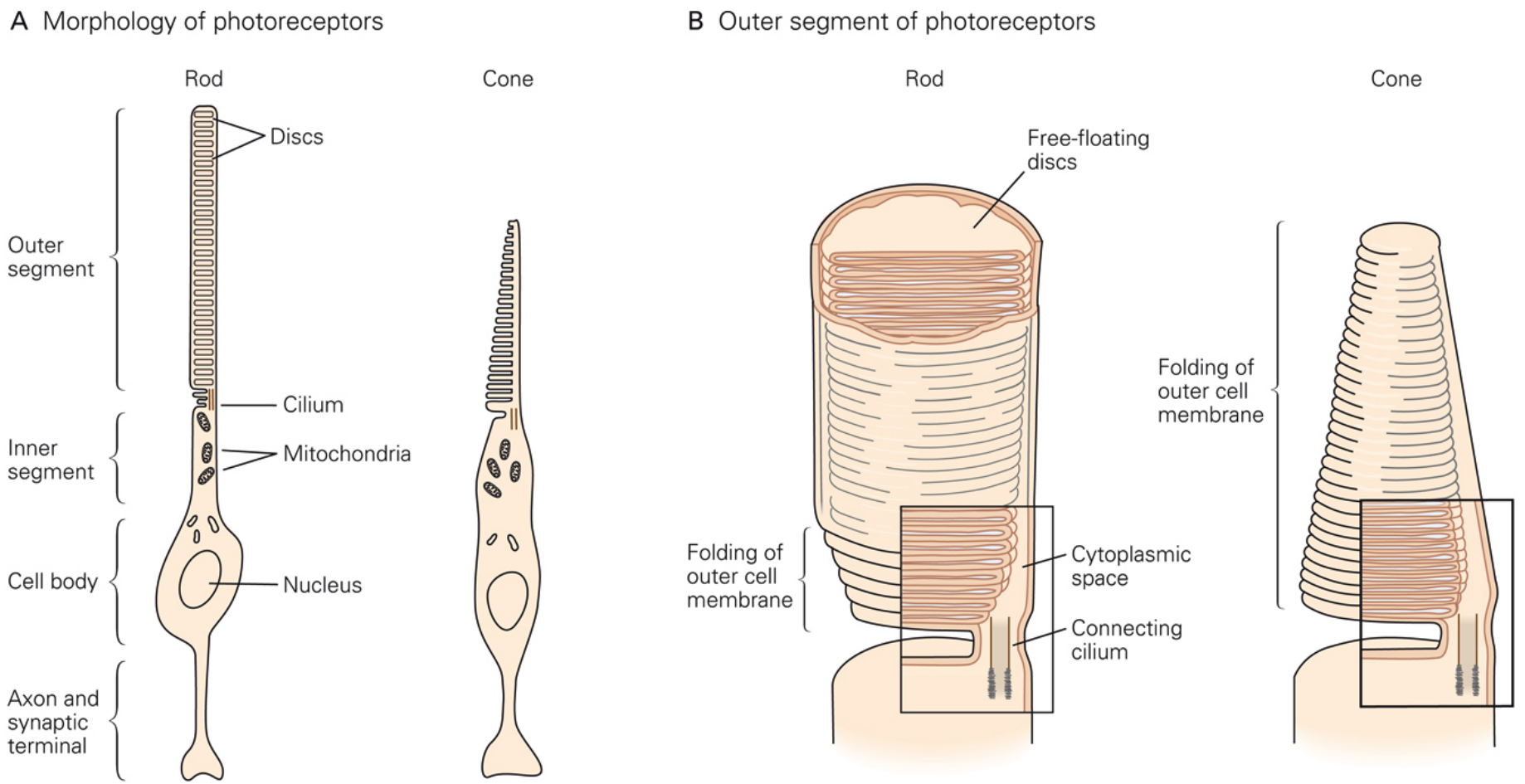

Figure 26–5 Rod and cone photoreceptors have similar structures.

A. Both rod and cone cells have specialized regions called the outer and inner segments. The outer segment, which is attached to the inner segment by a cilium, contains the light-transducing apparatus. The inner segment holds mitochondria and much of the machinery for protein synthesis.

B. The outer segment consists of a stack of membranous discs that contain the light-absorbing photopigments. In both types of cells these discs are formed by infolding of the plasma membrane. In rods, however, the folds pinch off from the membrane so that the discs are free-floating within the outer segment, whereas in cones the discs remain part of the plasma membrane. (Adapted, with permission, from O'Brien 1982; and Young 1970.)

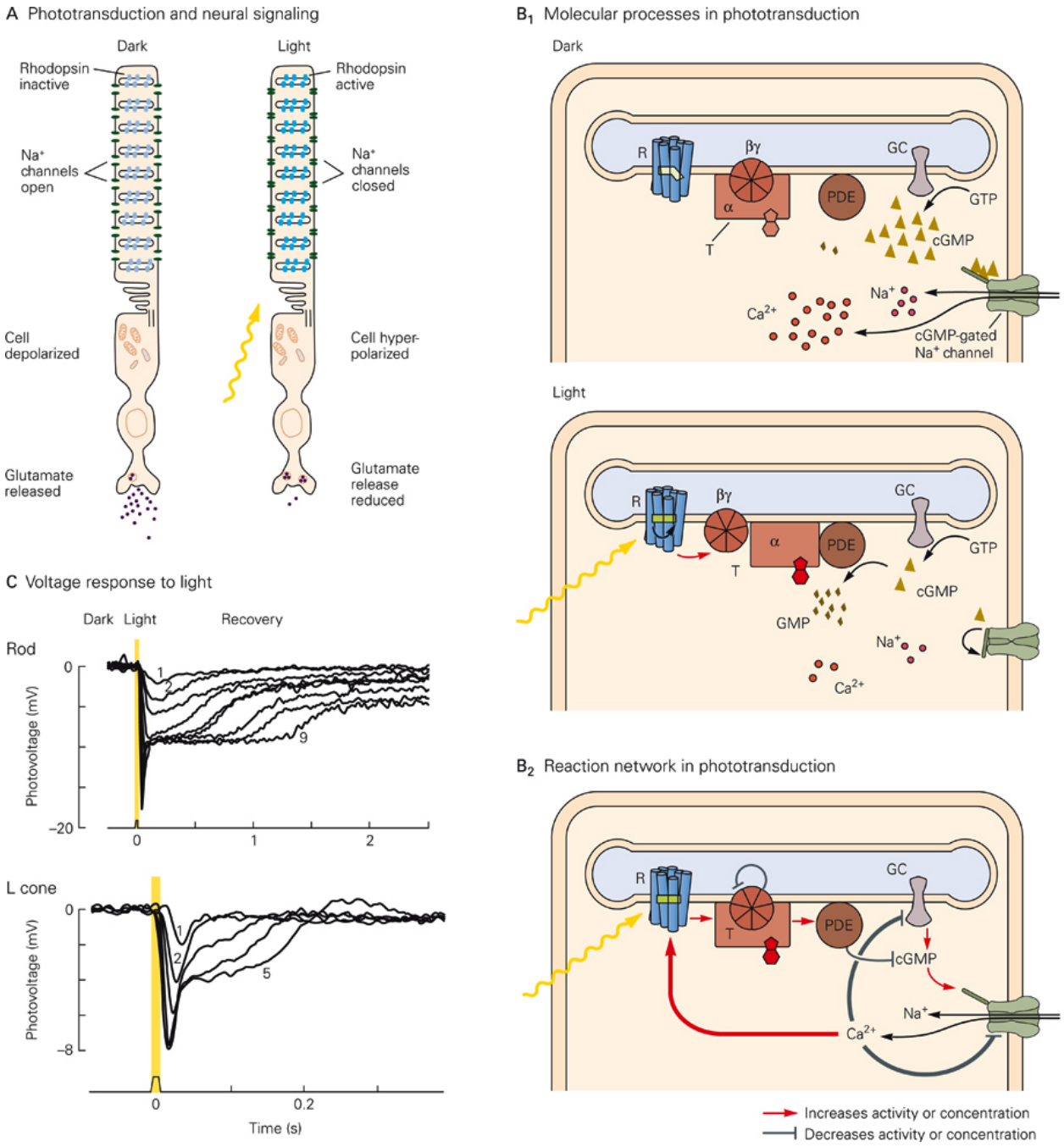

Figure 26–7 (Opposite) Phototransduction.

A. The rod cell responds to light. Rhodopsin molecules in the outer-segment discs absorb photons, which leads to the closure of cGMP-gated channels in the plasma membrane. This channel closure hyperpolarizes the membrane and reduces the rate of release of the neurotransmitter glutamate. (Adapted, with permission, from Alberts 2008.)

B. 1. Cyclic GMP (cyclic guanosine 3′-5′ monophosphate) is produced by a guanylate cyclase (**GC**) and hydrolyzed by a phosphodiesterase (**PDE**). In the dark the phosphodiesterase activity is low, the cGMP concentration is high, and the cGMP-gated channels are open, allowing the influx of Na^+ and Ca^{2+}. In the light rhodopsin (**R**) is excited by absorption of a photon, then activates transducin (**T**), which in turn activates the phosphodiesterase; the cGMP level drops, the membrane channels close, and less Na^+ and Ca^{2+} enter the cell. The transduction enzymes are all located in the internal membrane discs, and the soluble ligand cGMP serves as a messenger to the plasma membrane.

2. Calcium ions have a negative feedback role in the reaction cascade in phototransduction. Stimulation of the network by light leads to the closure of the cGMP-gated channels. This causes a drop in the intracellular concentration of Ca^{2+}. Because Ca^{2+} modulates the function of at least three components of the cascade—rhodopsin, guanylyl cyclase, and the cGMP-gated channel—the drop in Ca^{2+} counteracts the excitation caused by light.

C. Voltage response of a primate rod and cone to brief flashes of light of increasing intensity. Higher numbers on the traces indicate greater intensities of illumination (not all traces are labeled). For dim flashes the response amplitude increases linearly with intensity. At high intensities the receptor saturates and remains hyperpolarized steadily for some time after the flash; this leads to the afterimages that we perceive after a bright flash. Note that the response peaks earlier for brighter flashes and that cones respond faster than rods. (Reproduced, with permission, from Schneeweis and Schnapf 1995.)

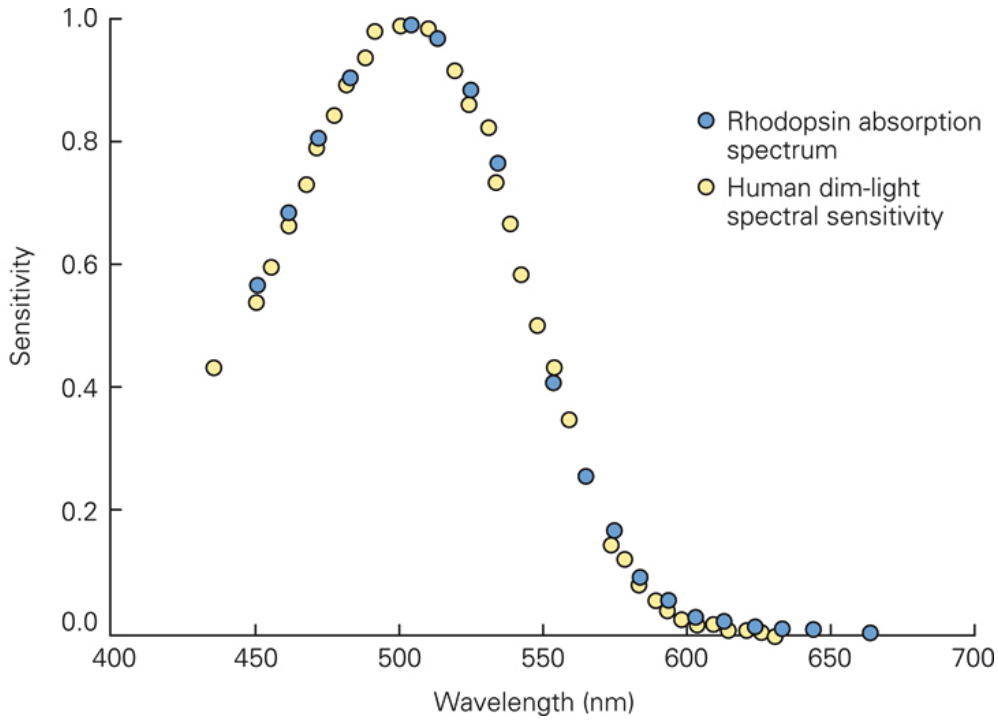

Figure 26–9 Absorption spectrum of rhodopsin. This plot compares the absorption spectrum of human rhodopsin measured in a cuvette and the spectral sensitivity of human observers to very dim light flashes. The psychophysical data have been corrected for absorption by the ocular media. (Reproduced, with permission, from Wald and Brown 1956.)

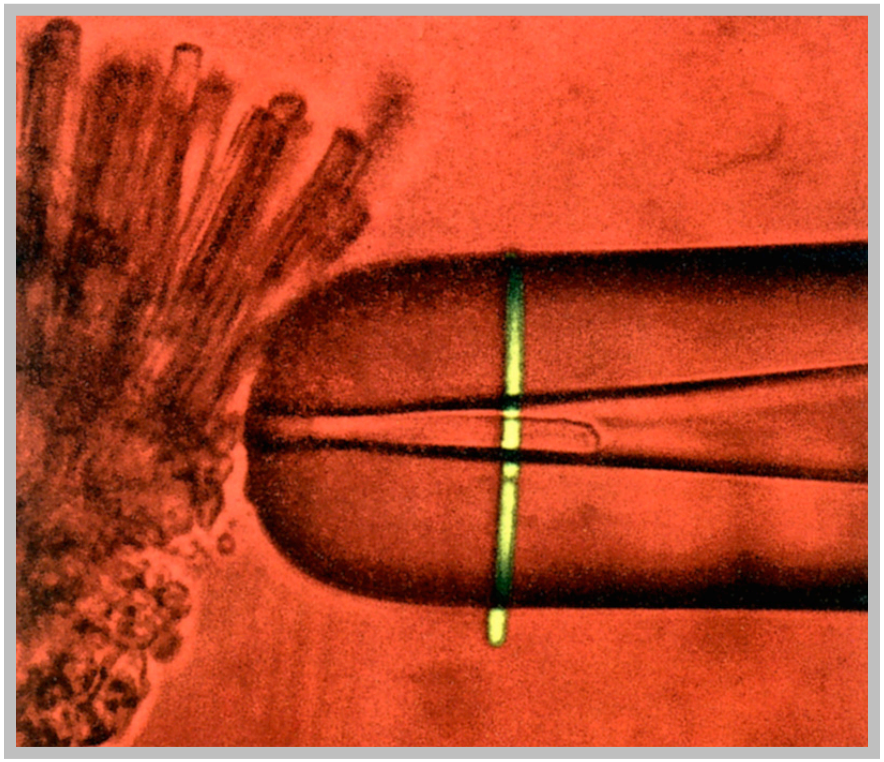

Suction electrode recording

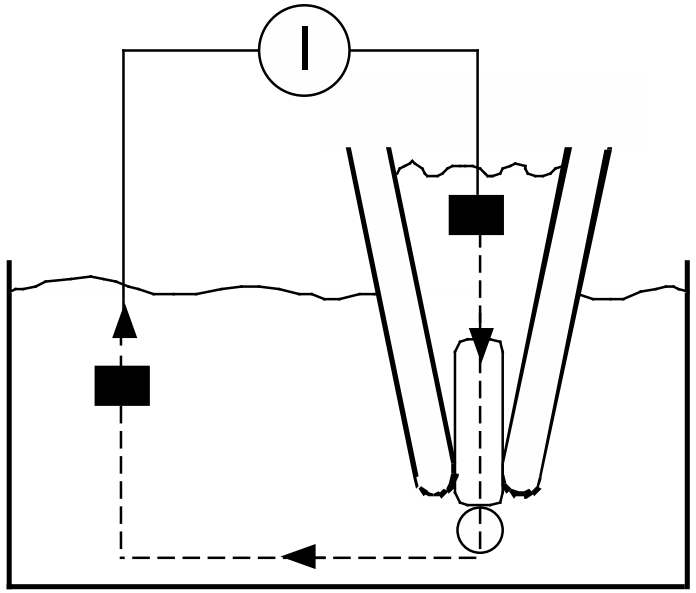

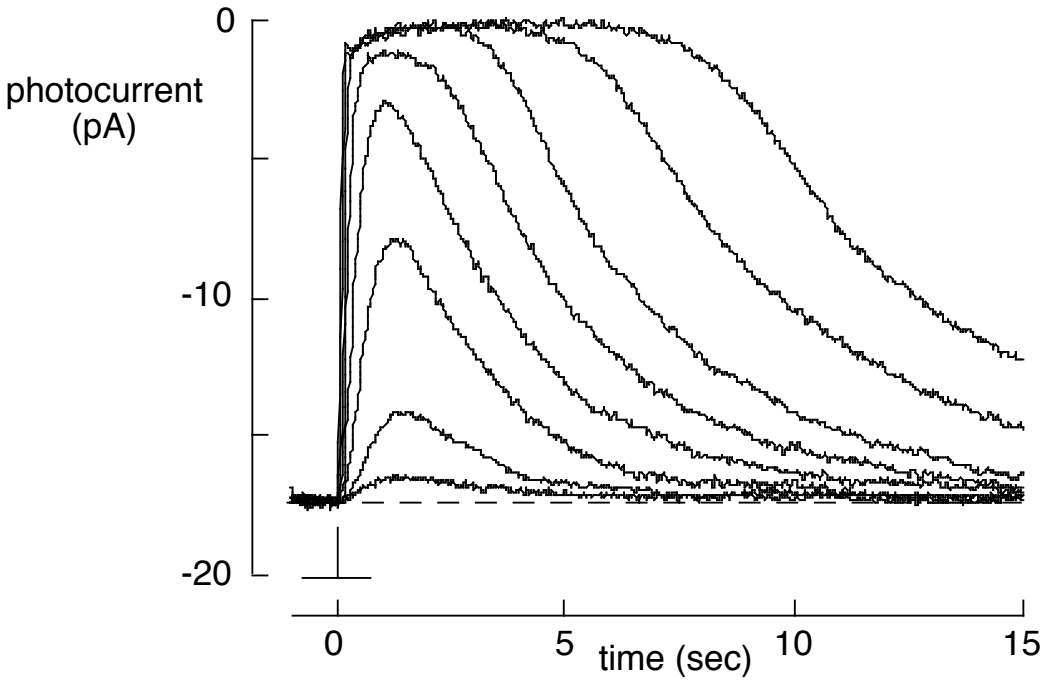

courtesy F. Rieke

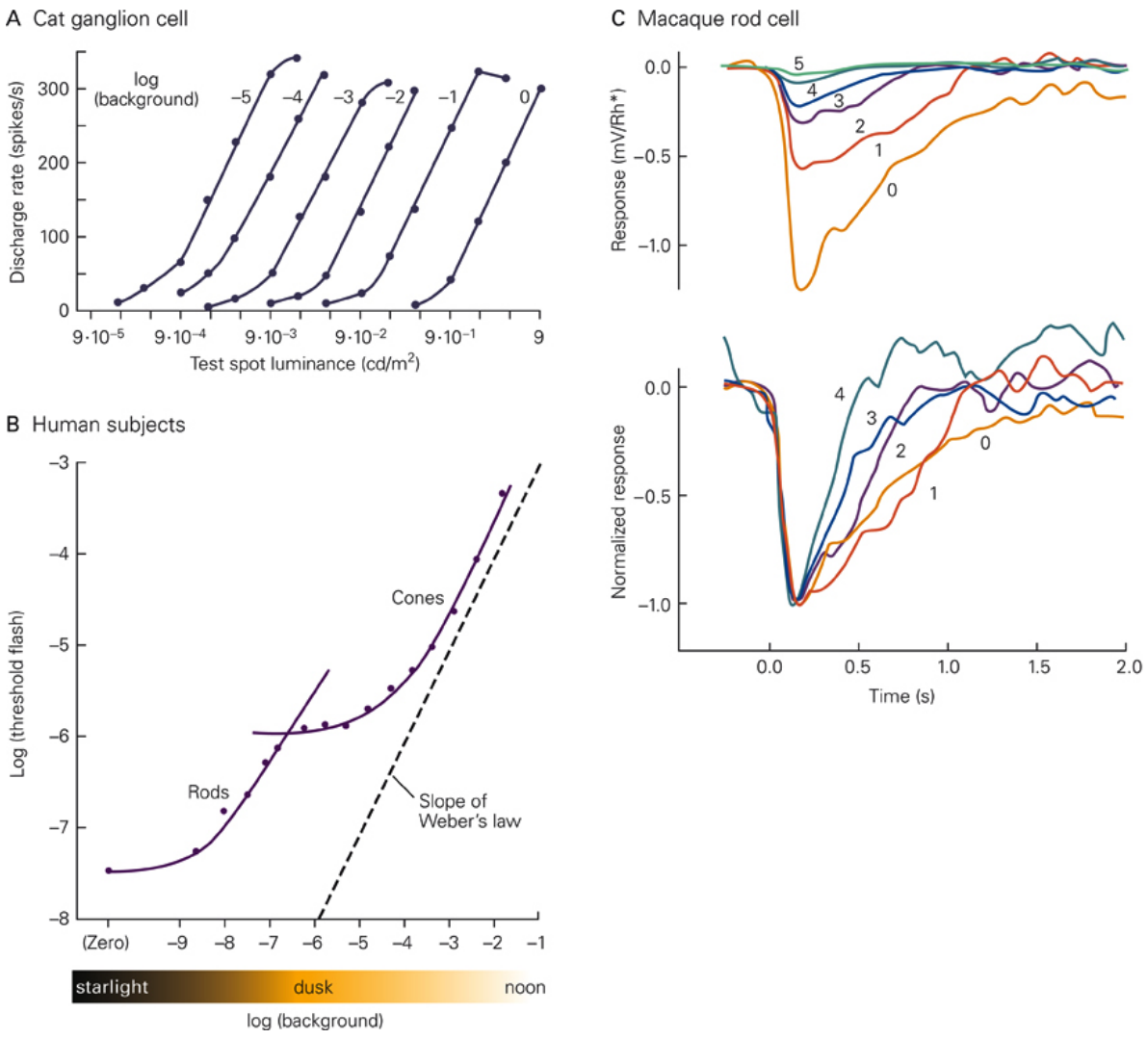

Figure 26–19 Light adaptation.

A. Light adaptation in a cat's retinal ganglion cell. The receptive field was illuminated uniformly at a steady background intensity, and a test spot was flashed briefly on the receptive field center. The peak firing rate following the flash was measured and plotted against the logarithm of the flash intensity. Each curve corresponds to a different background intensity, increasing by factors of 10 from left to right. (Reproduced, with permission, from Sakmann and Creutzfeldt 1969.)

B. Light adaptation in human vision. A small test spot was flashed briefly on a steadily illuminated background, and the intensity at which human subjects just detected the flash is plotted against the background intensity. The curve has two branches connected by a distinct kink: These correspond to the regimes of rod-and-cone vision. The slope of Weber's law represents the idealization in which the threshold intensity is proportional to the background intensity. (Reproduced, with permission, from Wyszecki and Stiles 1967.)

C. Light adaptation in the macaque monkey. The top plot shows the responses of a macaque monkey's rod cell to flashes delivered at varying background intensities. The cell's single-photon response was calculated from the recorded membrane potential divided by the number of rhodopsins (Rh) activated by the flash. The gain of the single-photon response decreases substantially with increasing background intensity. The background intensity, in photon/μm^2/s, is 0 for trace 0, 3.1 for trace 1, 12 for trace 2, 41 for trace 3, 84 for trace 4, and 162 for trace 5. In the bottom plot the same data (except for the smallest response) are normalized to the same amplitude, showing that the time course of the single-photon response accelerates at high intensity. (Reproduced, with permission, from Schneeweis and Schnapf 2000.)

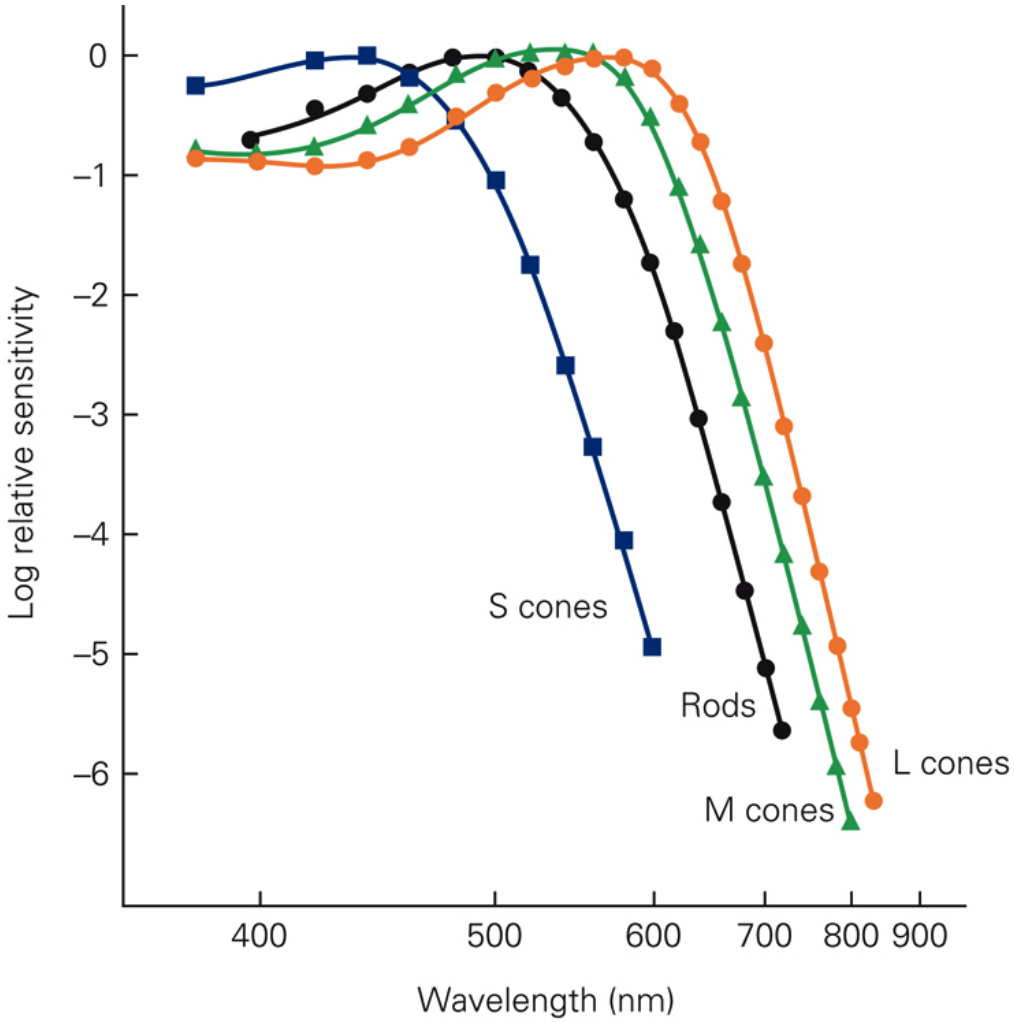

Figure 26–6 Sensitivity spectra for the three cones and the rod. At each wavelength the sensitivity is inversely proportional to the intensity of light required to elicit a criterion neural response. Sensitivity varies over a large range and thus is shown on a logarithmic scale. The different classes of photoreceptors are sensitive to broad and overlapping ranges of wavelengths. (Reproduced, with permission, from Schnapf et al. 1988.)

Photoreceptor Response Univariance

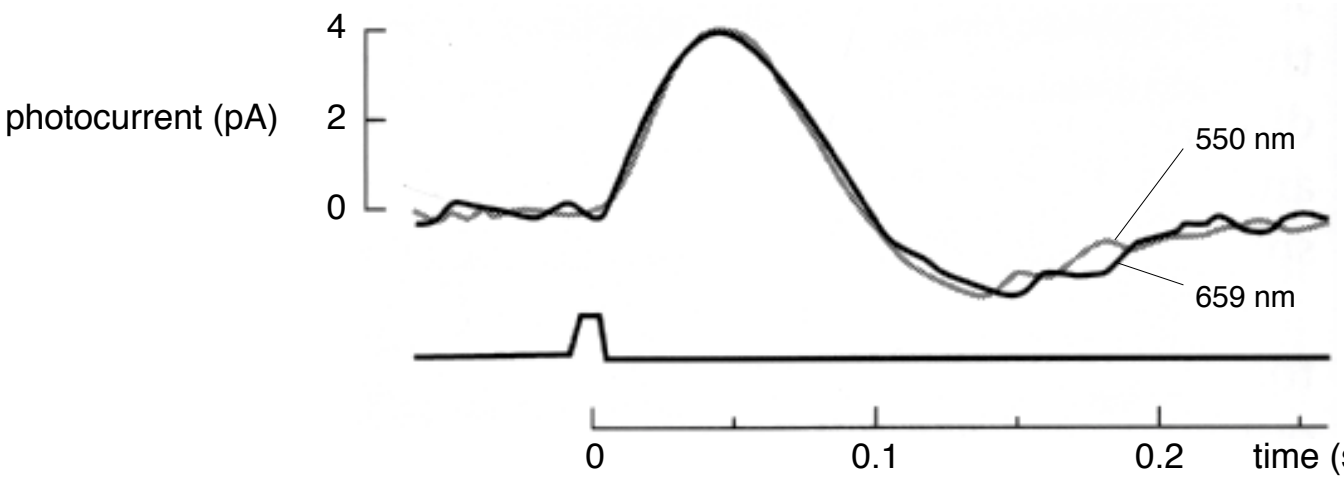

Baylor et al (1987)

Number of photons absorbed determines photoreceptor response
so one photoreceptor type cannot signal wavelength

Mosaic of Red, Green and Blue Cones of the Living Human Retina

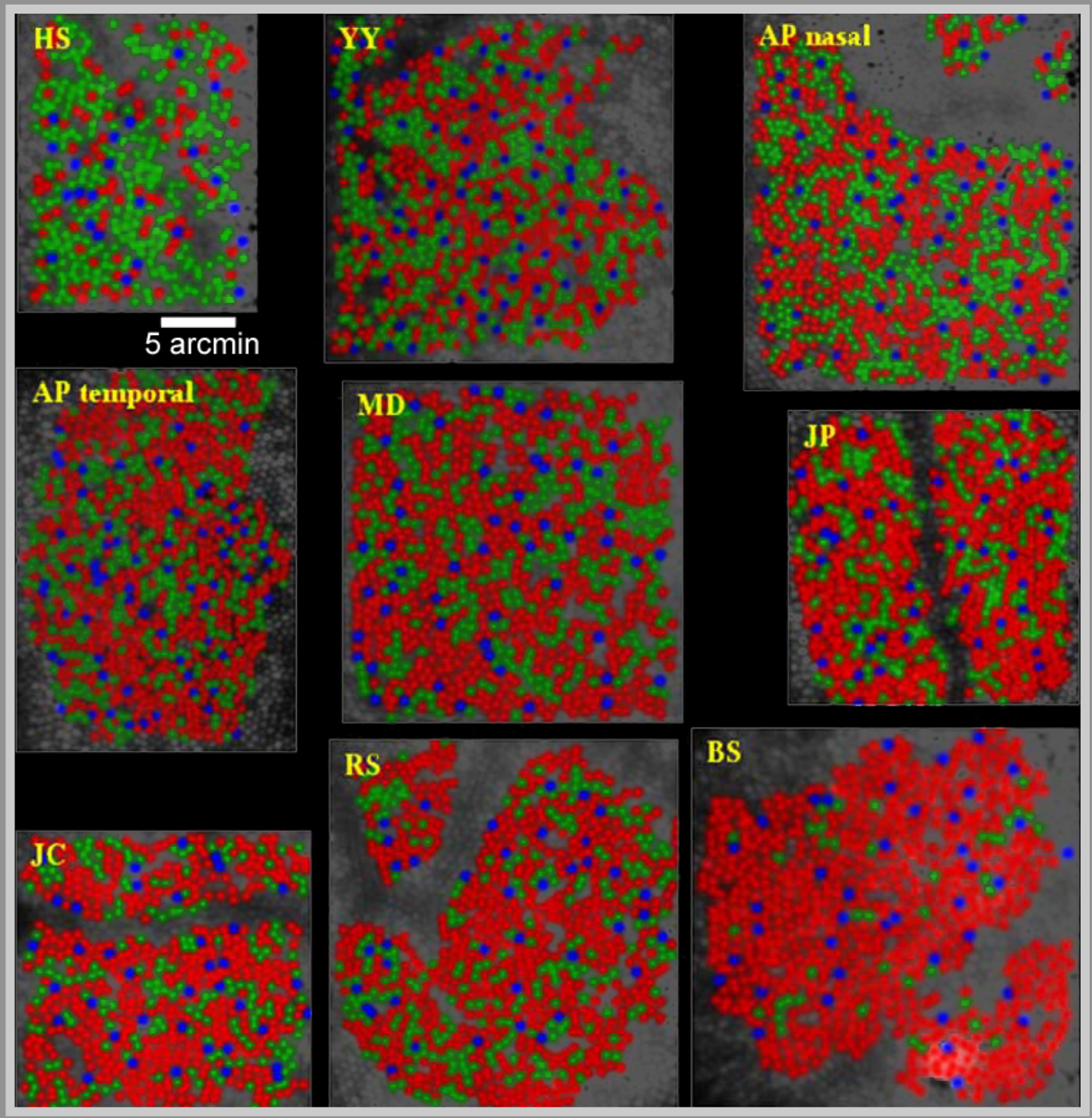

Hofer et al. (2005)

Adaptation in Primate Cones

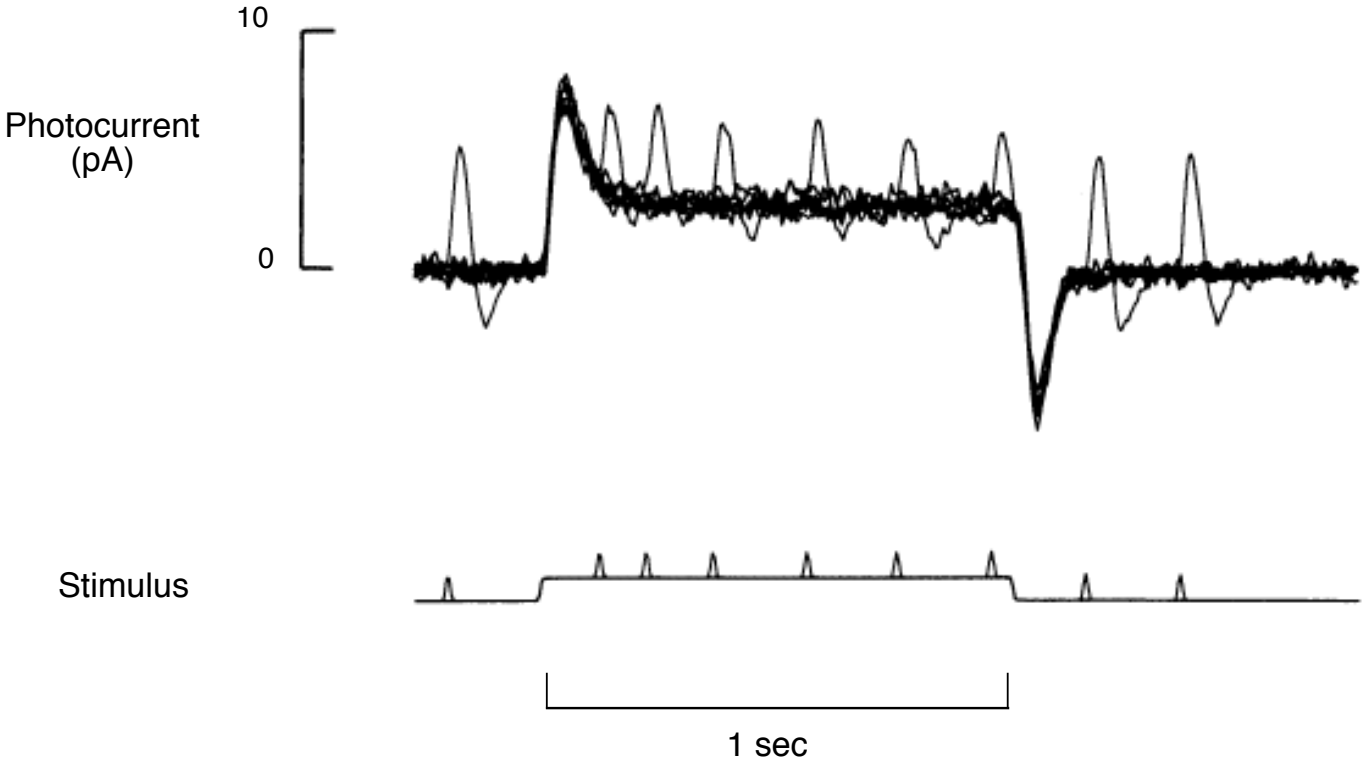

Schnapf et al (1990)

Adaptation in primate cones

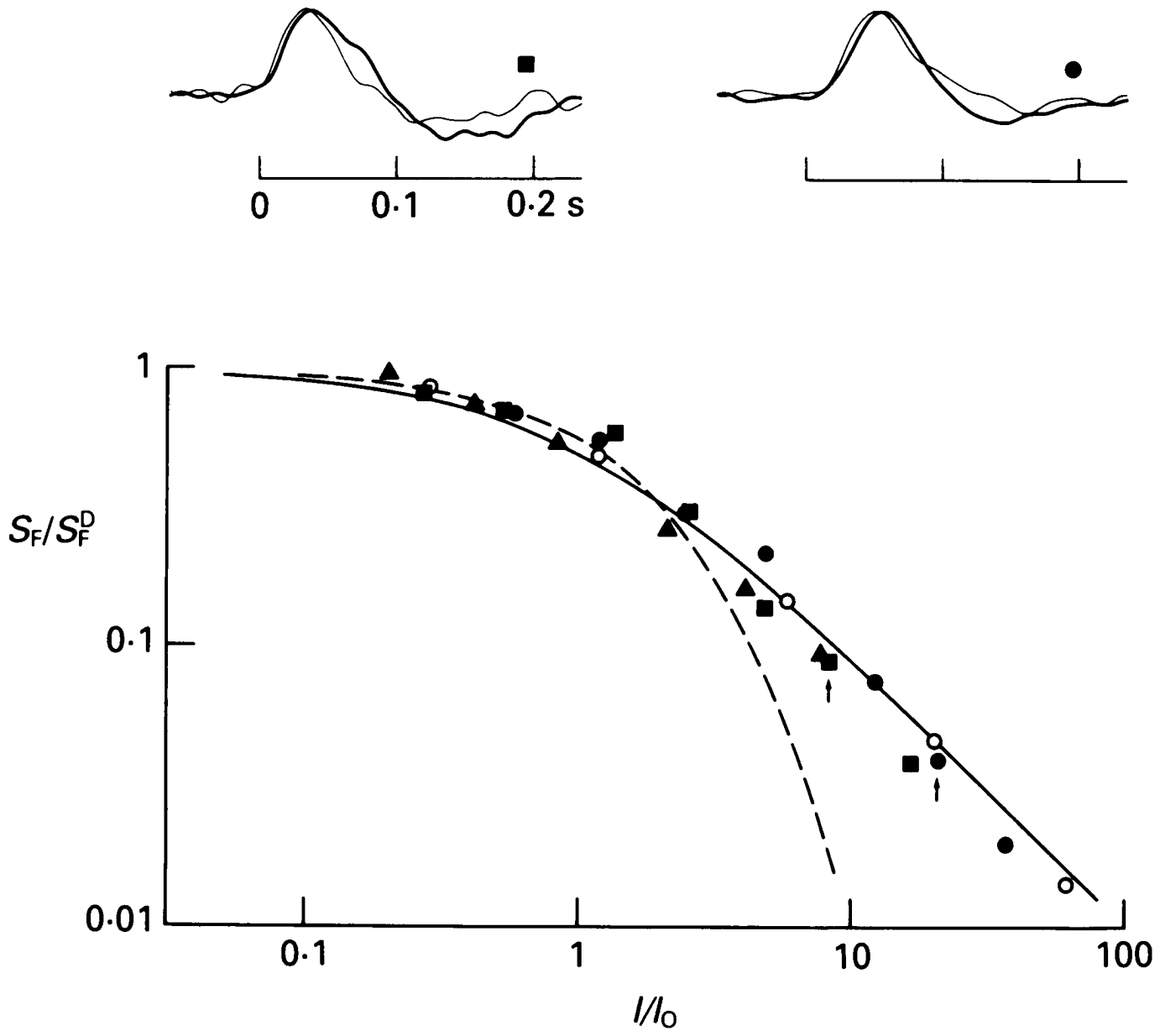

Retinal cell type diversity and circuit specificity

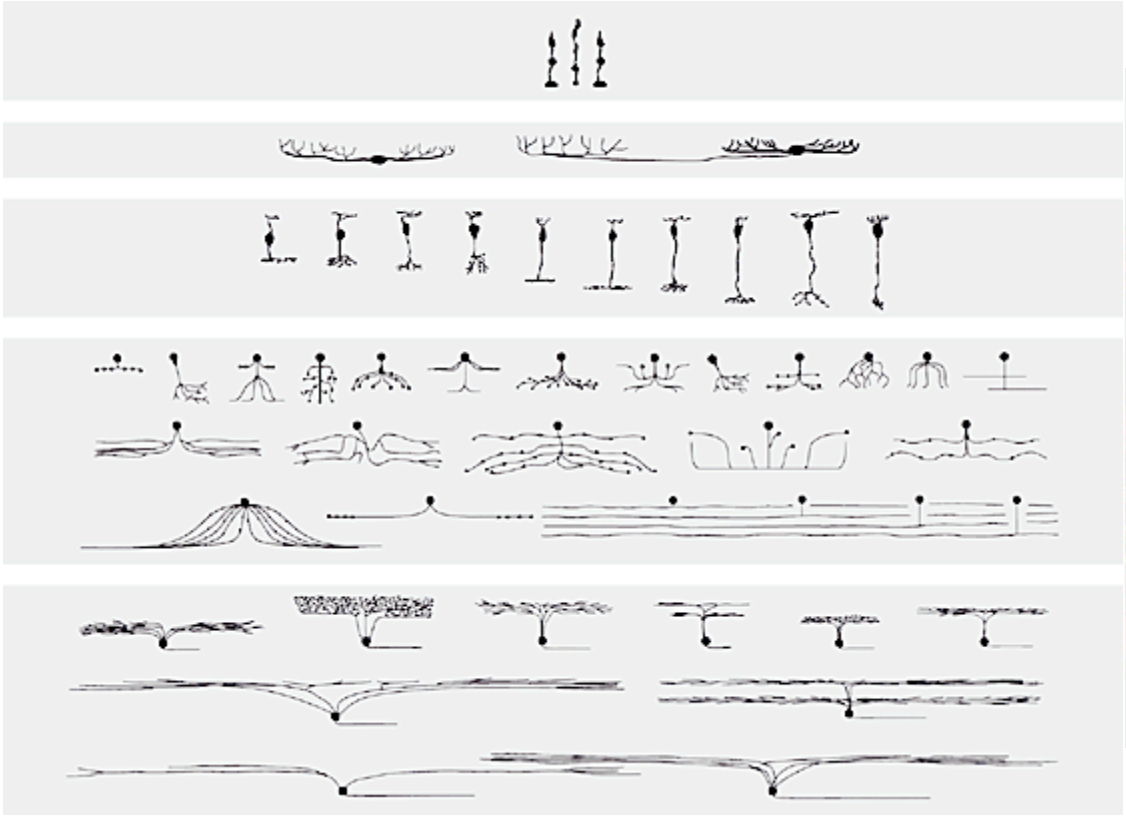

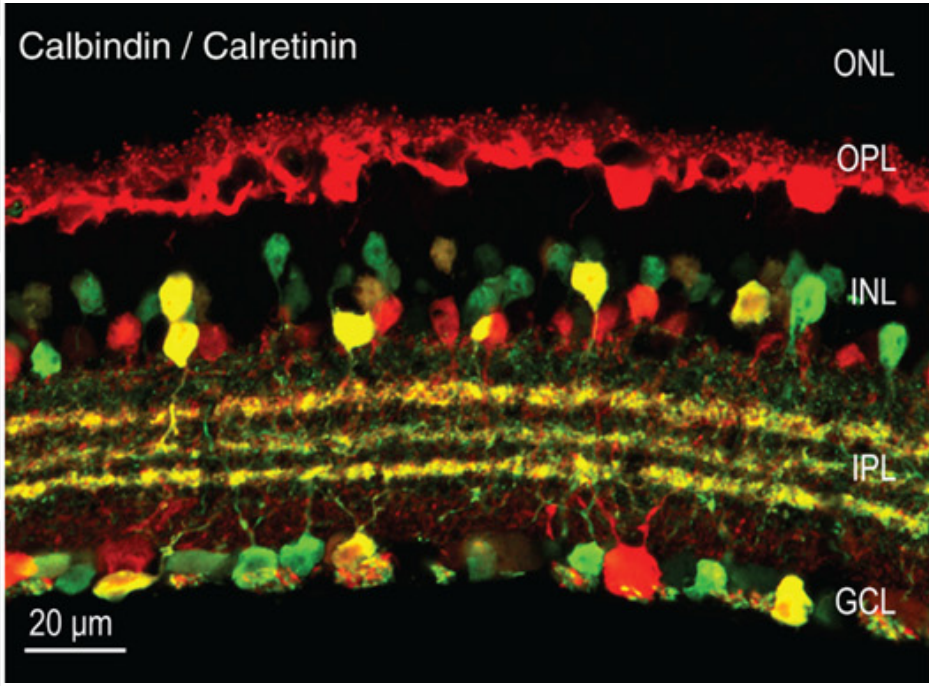

Masland, 2001

On and off bipolar cells

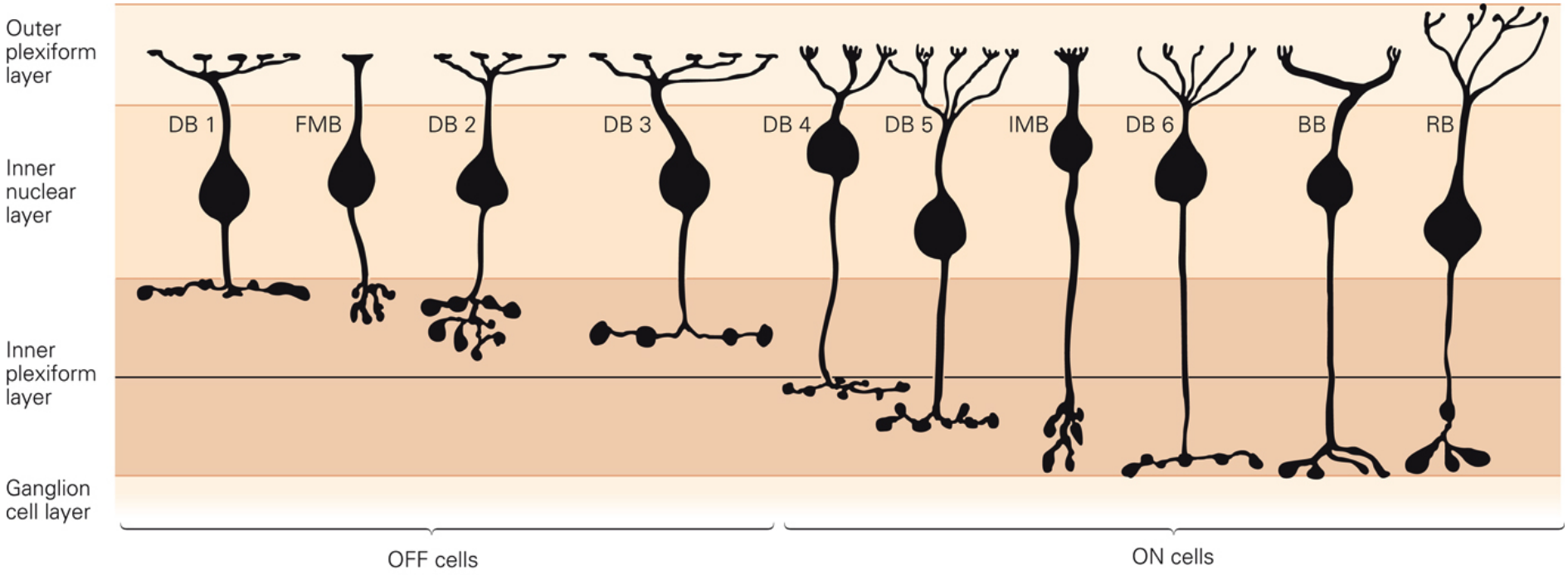

Figure 26–15 Bipolar cells in the macaque retina. The cells are arranged according to the depth of their terminal arbors in the inner plexiform layer. The horizontal line dividing the distal and proximal levels of this layer represents the border between the axonal terminals of OFF and ON types. Bipolar cells with axonal terminals in the upper (distal) half are presumed to be OFF cells, those in the lower (proximal) half ON cells. Cell types are diffuse bipolar cells (**DB**), ON and OFF midget bipolars (**IMB, FMB**), S-cone ON bipolar (**BB**), and rod bipolar (**RB**). (Reproduced, with permission, from Boycott and Wässle 1999.)

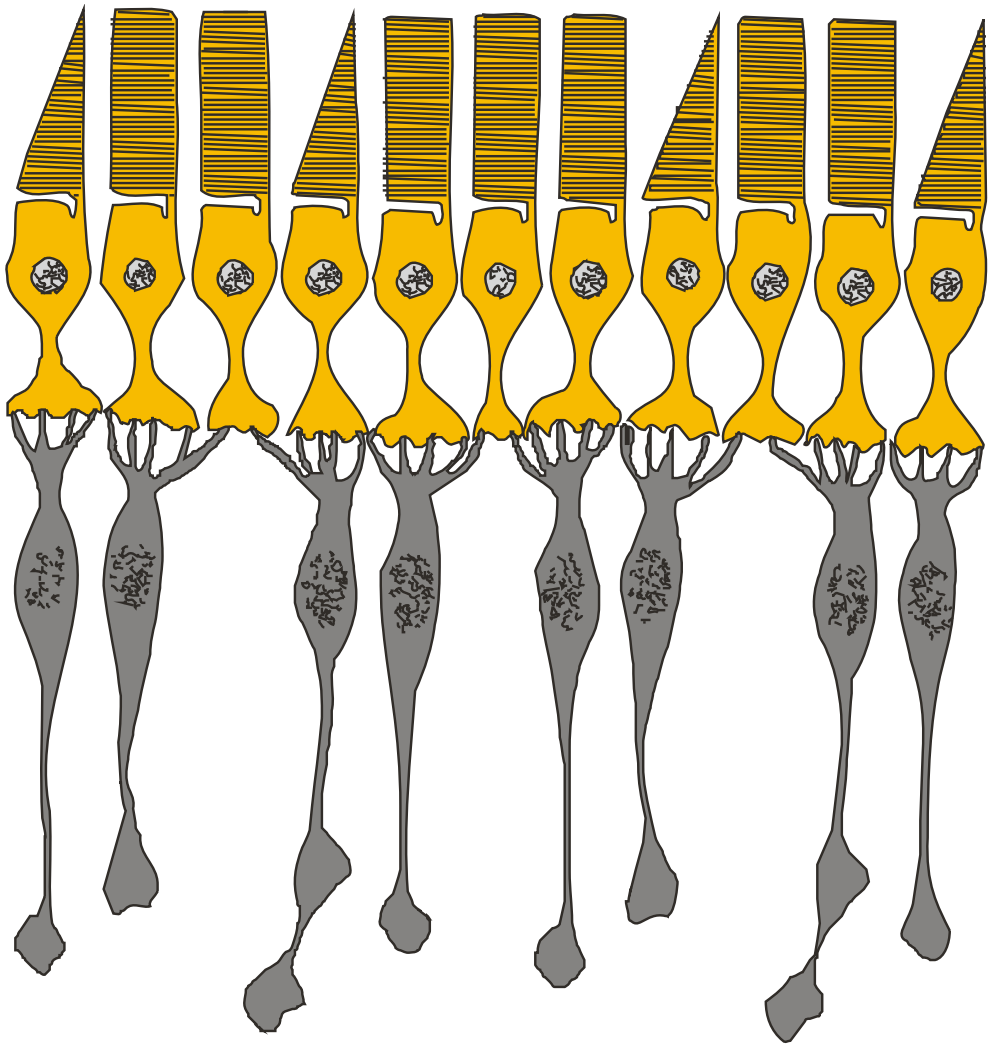

Photoreceptors

Bipolar Cells

Light

Outputs from cones

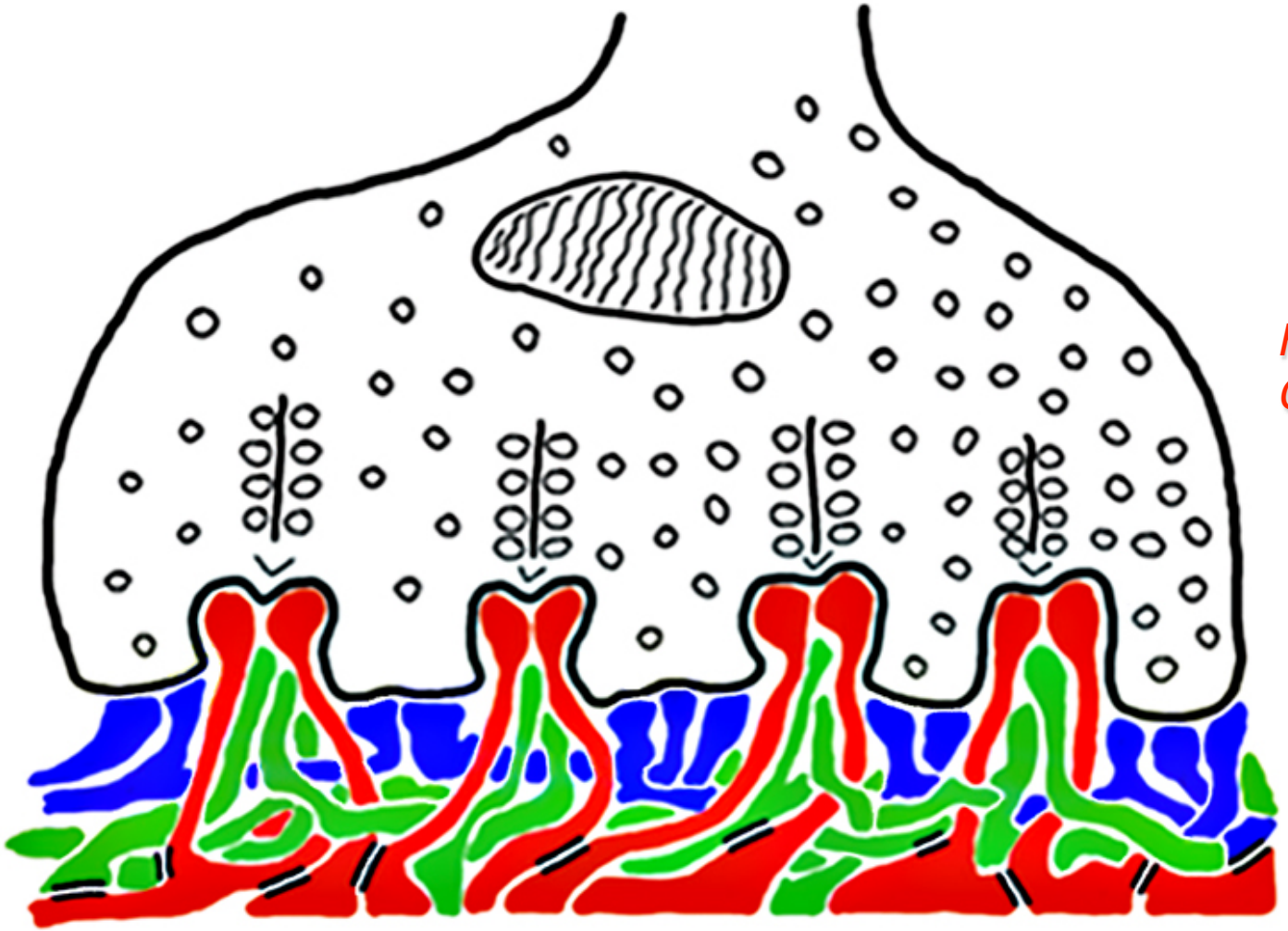

Horizontal Cells: 2 types

ON - Bipolar Cells: 4 types

OFF - Bipolar Cells: 4 types

Outputs from cones

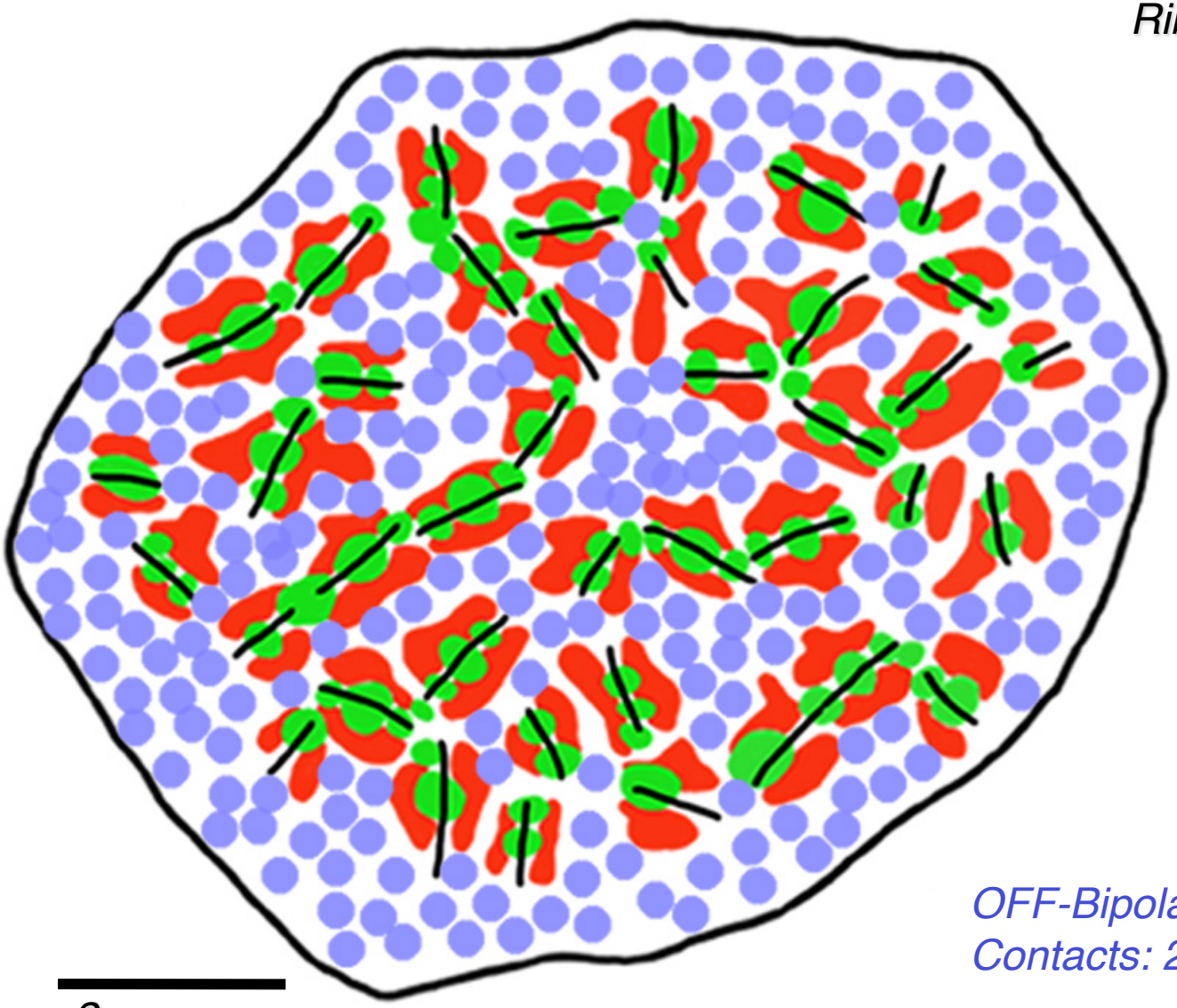

Ribbons: 39

Horizontal Cell
Contacts: 80

ON-Bipolar Cell
Contacts: 90

OFF-Bipolar Cell
Contacts: 200-300

2 µm

On and off bipolar cells

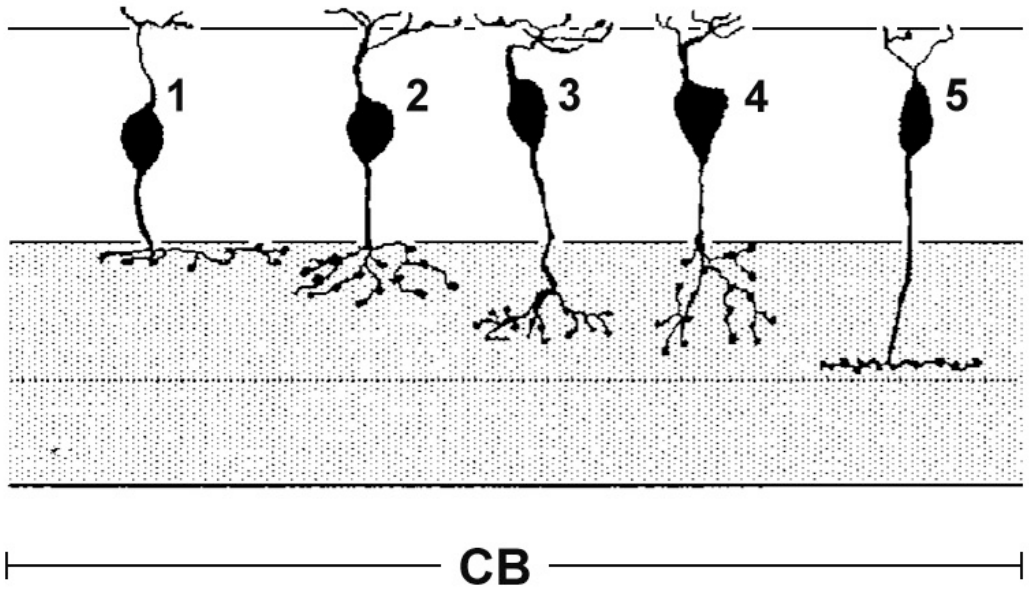

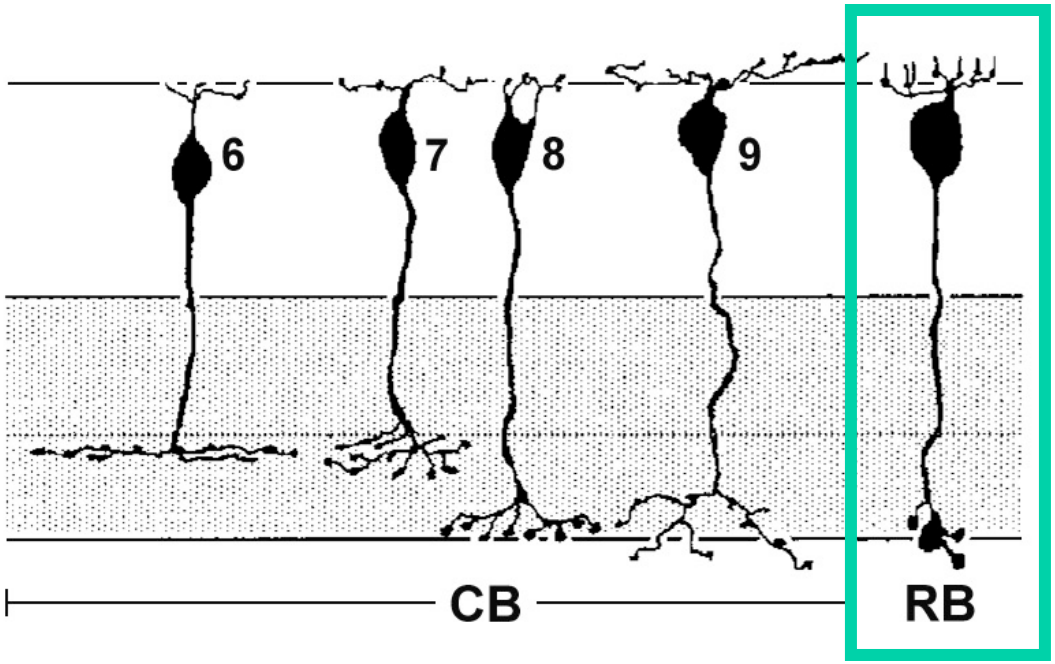

OFF Bipolar Cells

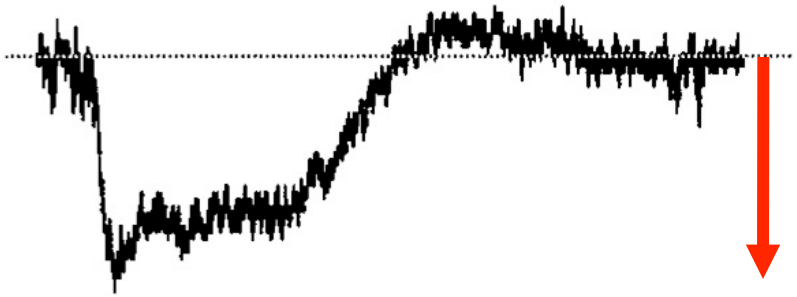

ON Bipolar Cells

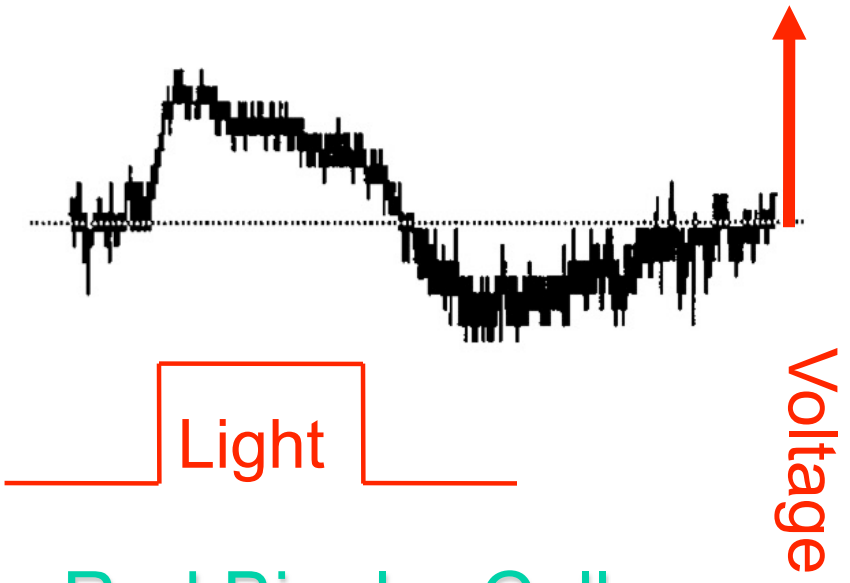

Rod Bipolar Cell

Outputs from cones

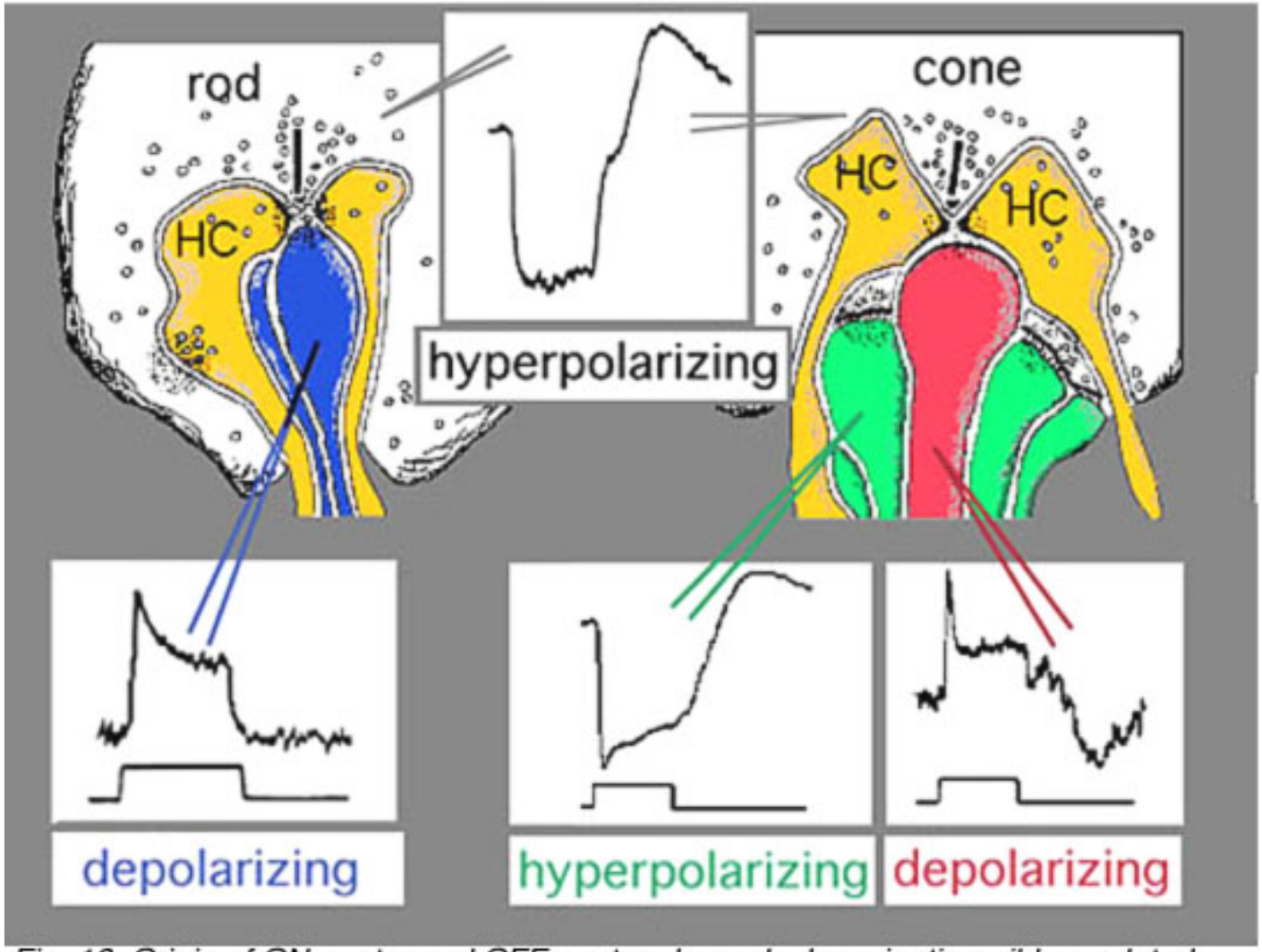

Fig. 16. Origin of ON-center and OFF-center channels. Invaginating, ribbon related contacts give rise to depolarizing responses; flat or basal contacts give rise to hyperpolarizing responses.

Outputs from cones

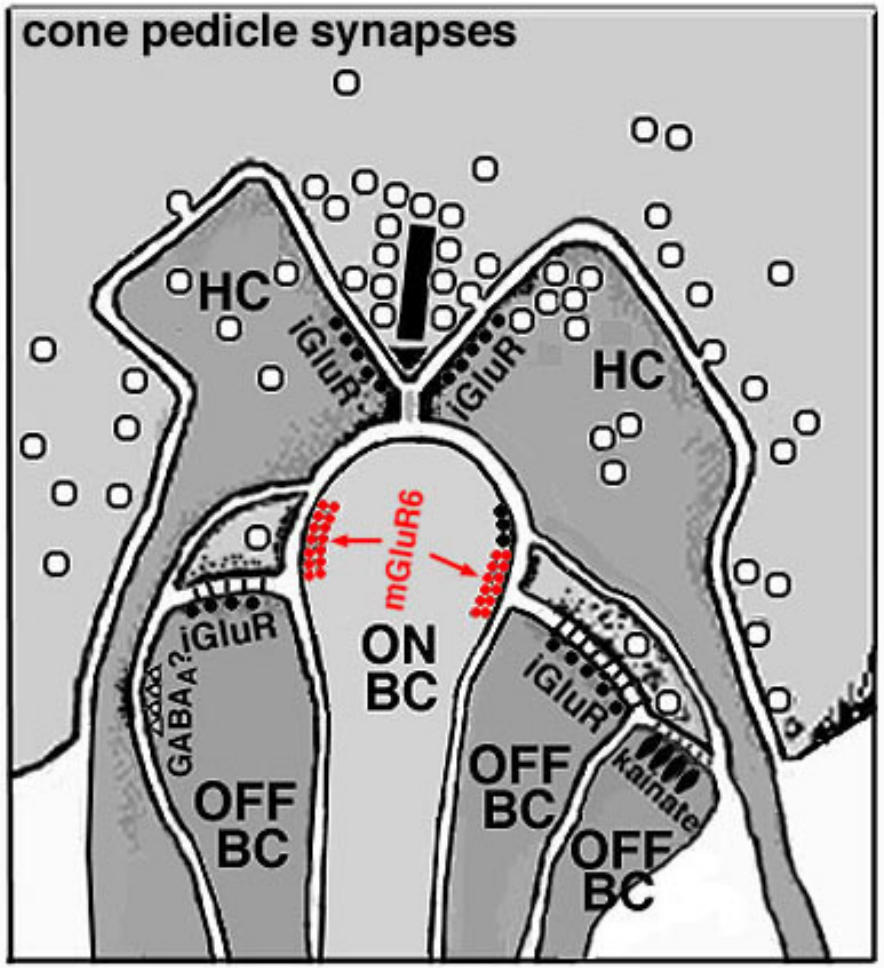

Fig. 17. Drawing of the organization of the photoreceptor synapse showing the different glutamate receptors that are presently known to be on the various postsynaptic dendrites.

Center-Surround Antagonism in Primate Bipolar Cells

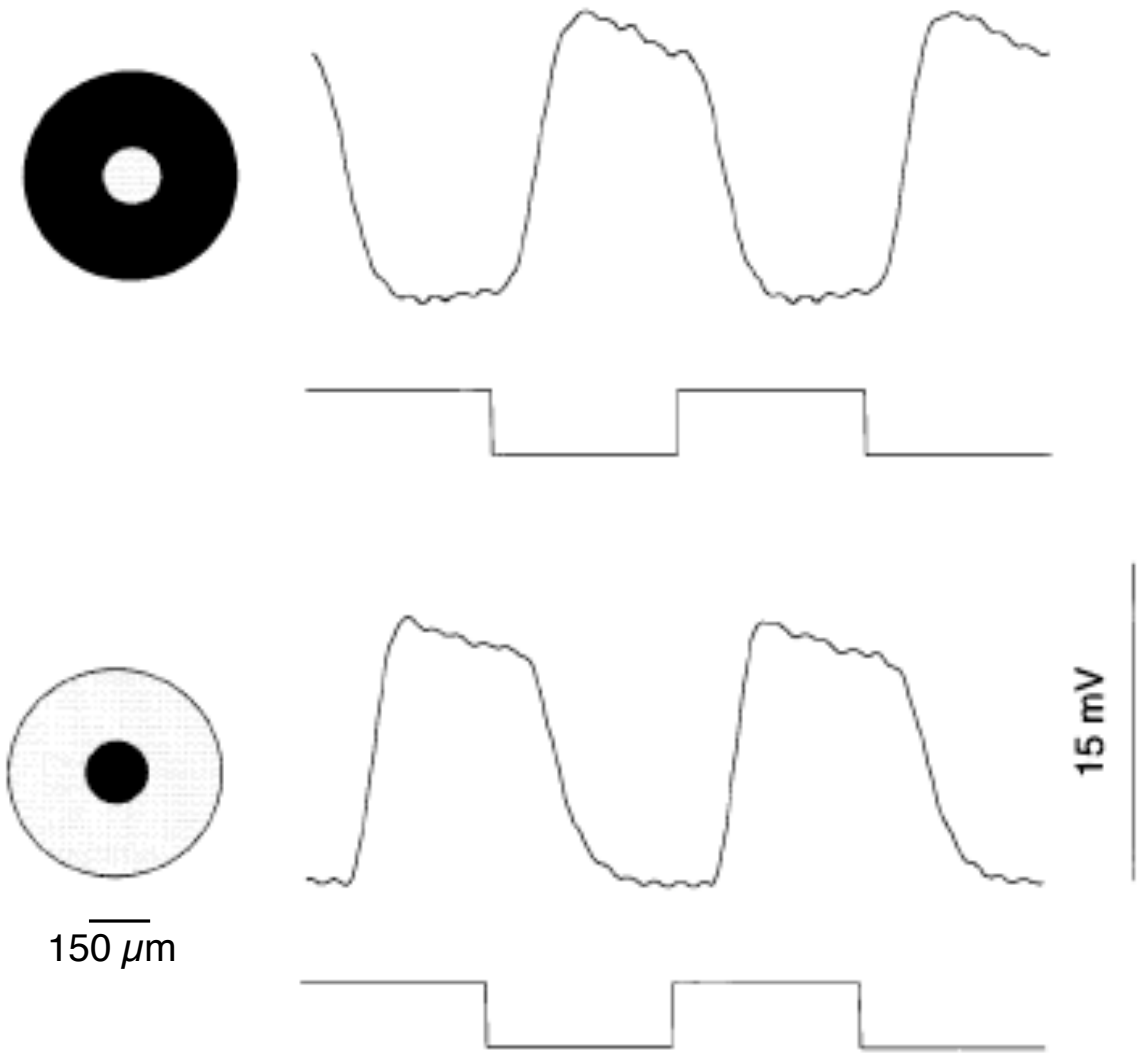

Dacey et al (2000)

Center-Surround Antagonism in Primate Cones

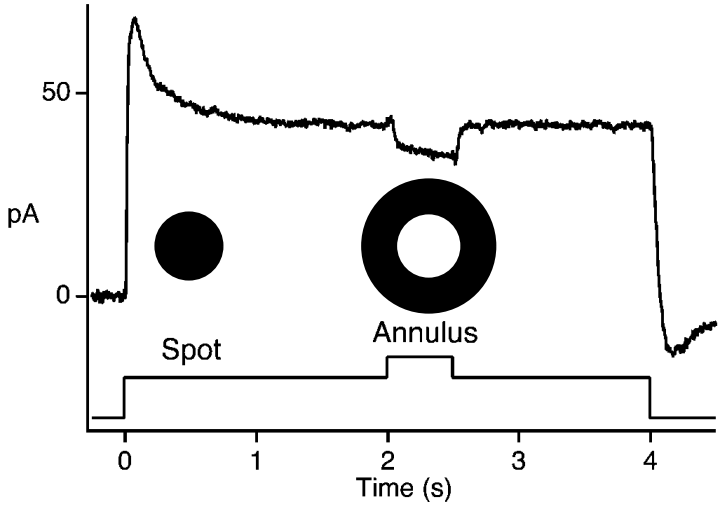

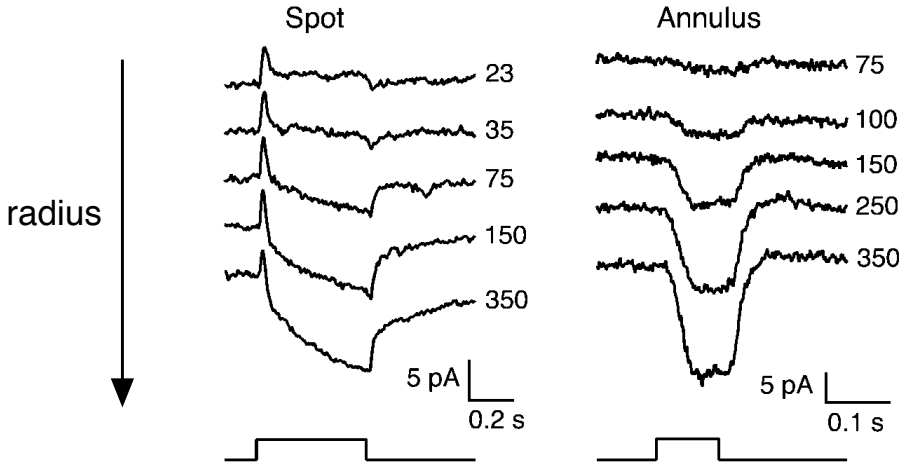

Verweij et al (2003)

Primate H1 Horizontal Cell Mosaic

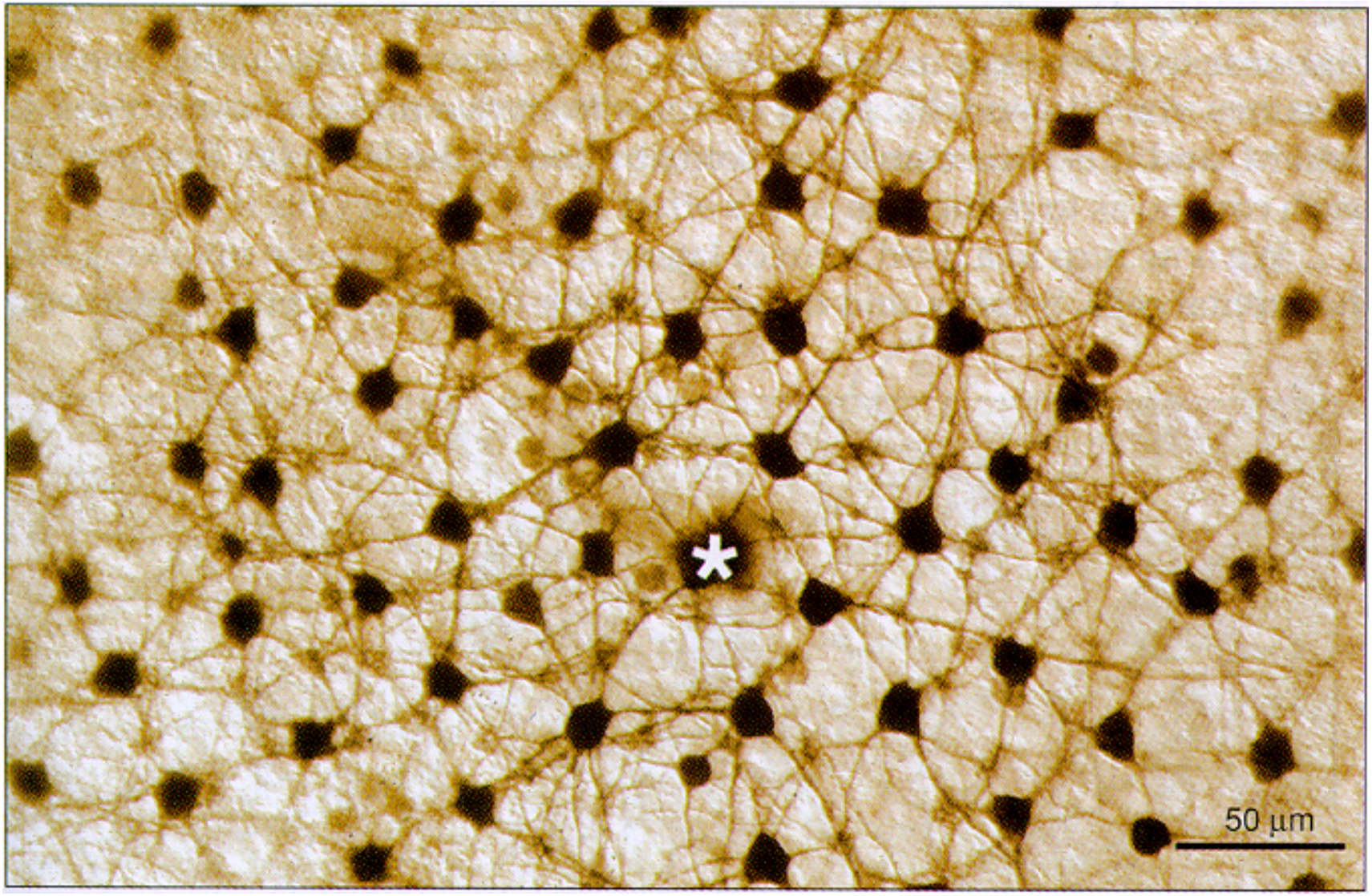

Dacey et al (1996)

The principal bipolar cell types of the primate retina

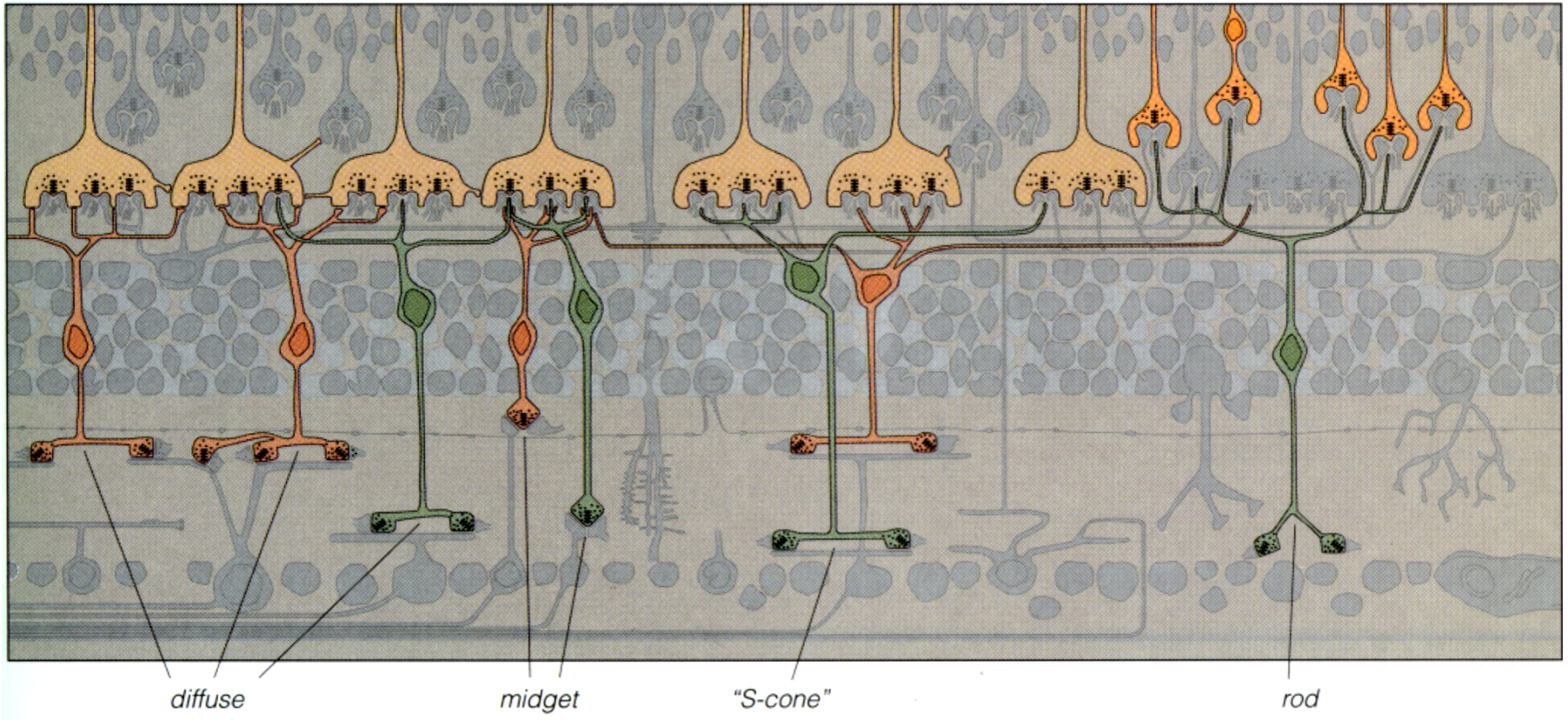

The principal ganglion cell types of the primate retina

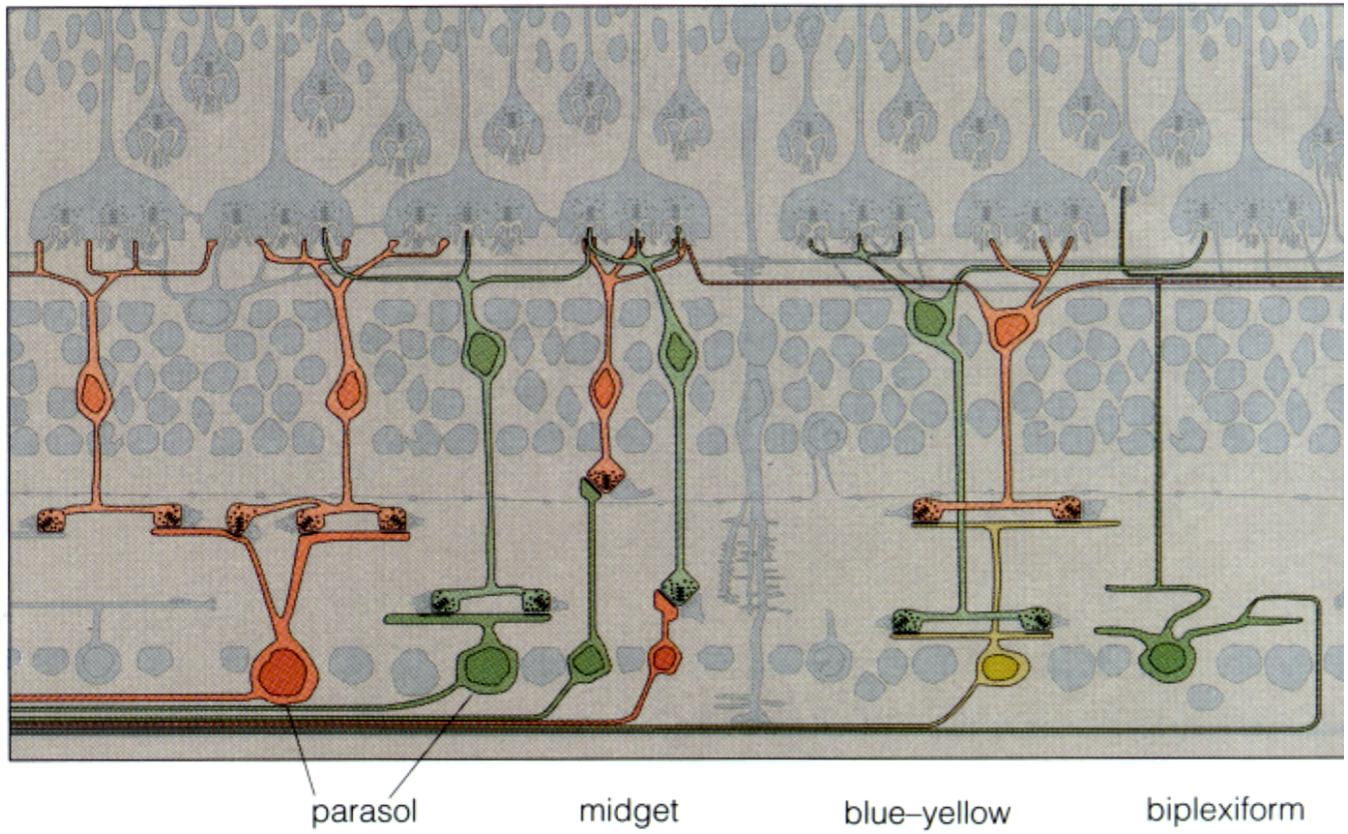

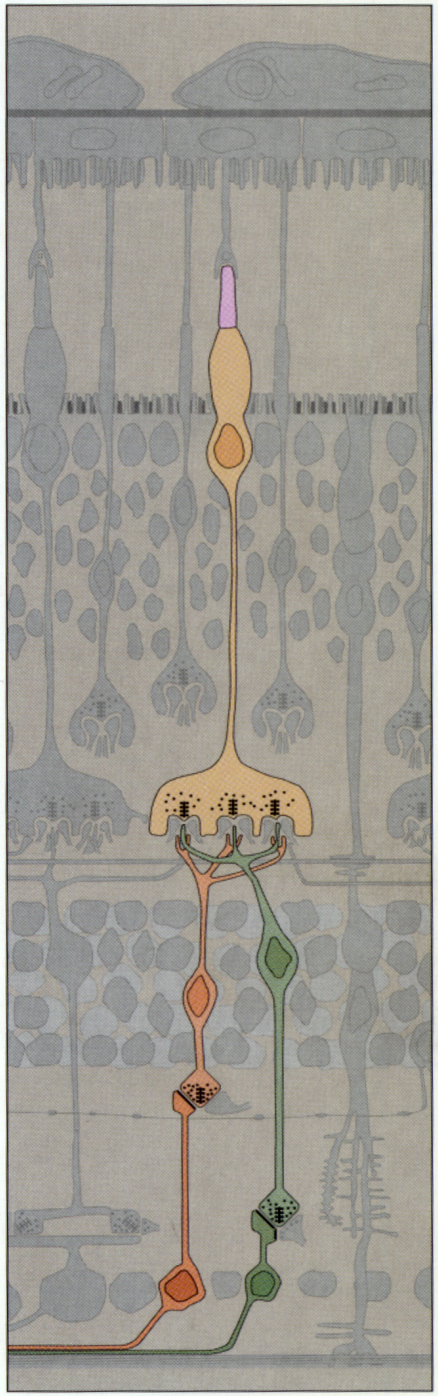

off- and on-midget pathways

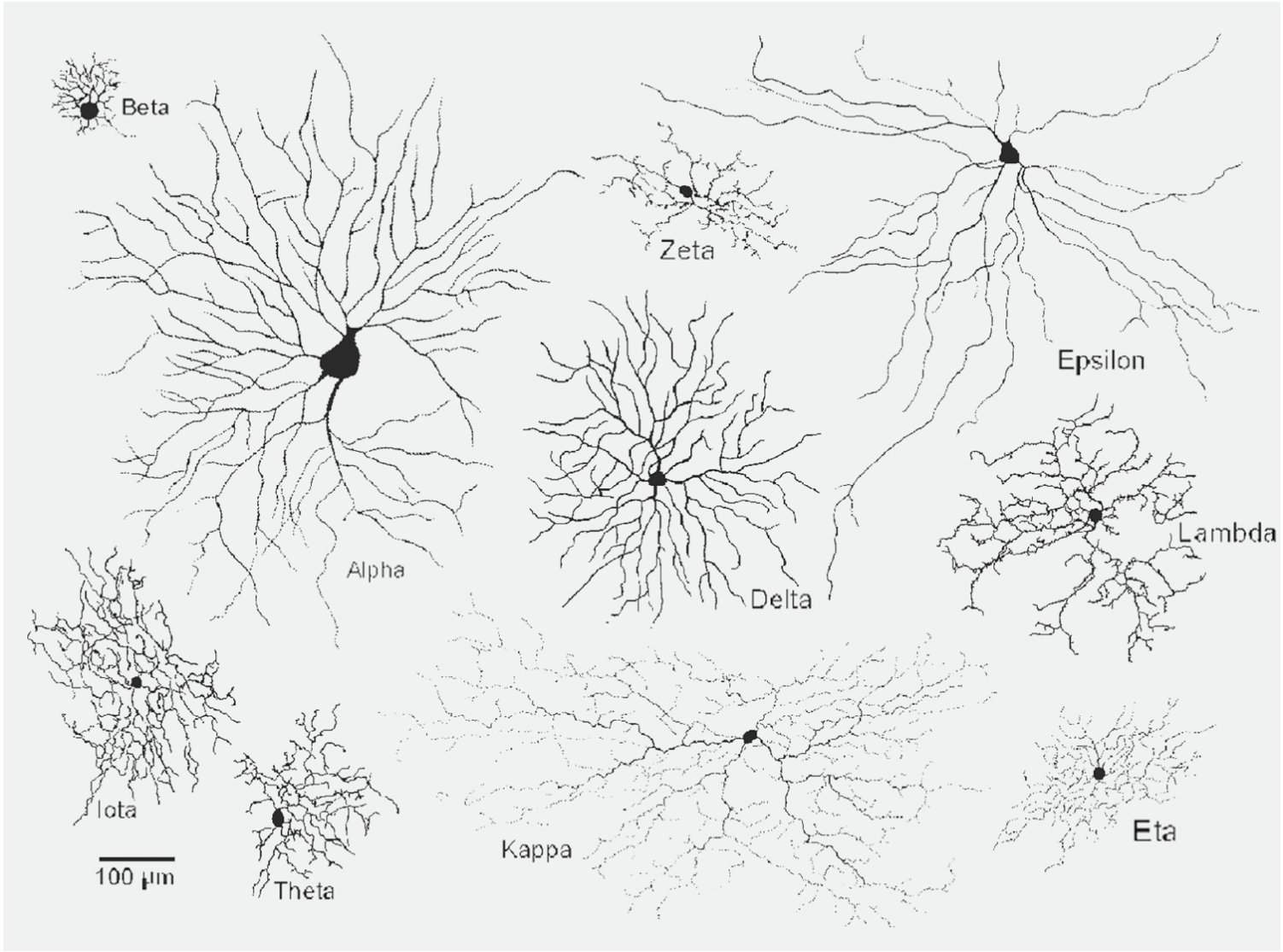

Fig. 5. The types of ganglion cells identified thus far in the retina of the cat. Ongoing work in the rabbit and monkey confirms this diversity, and many of the cells observed are probably homologs of those seen in the cat. Courtesy of D. Berson[77–80].

Masland, 2001

Retinal Ganglion Cell Mosaic

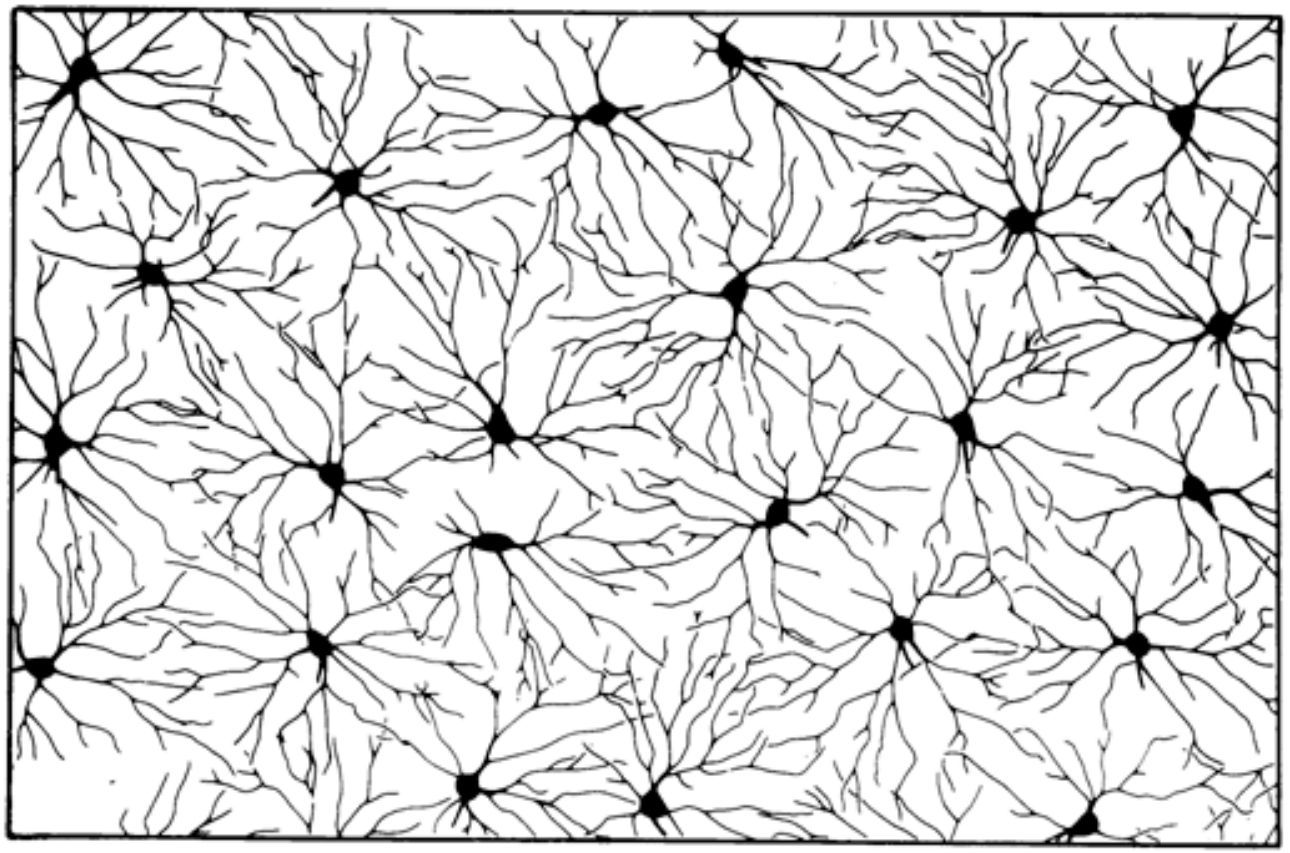

Wassle et al (1981)

Midget Retinal Ganglion Cell Dendritic Field Mosaic

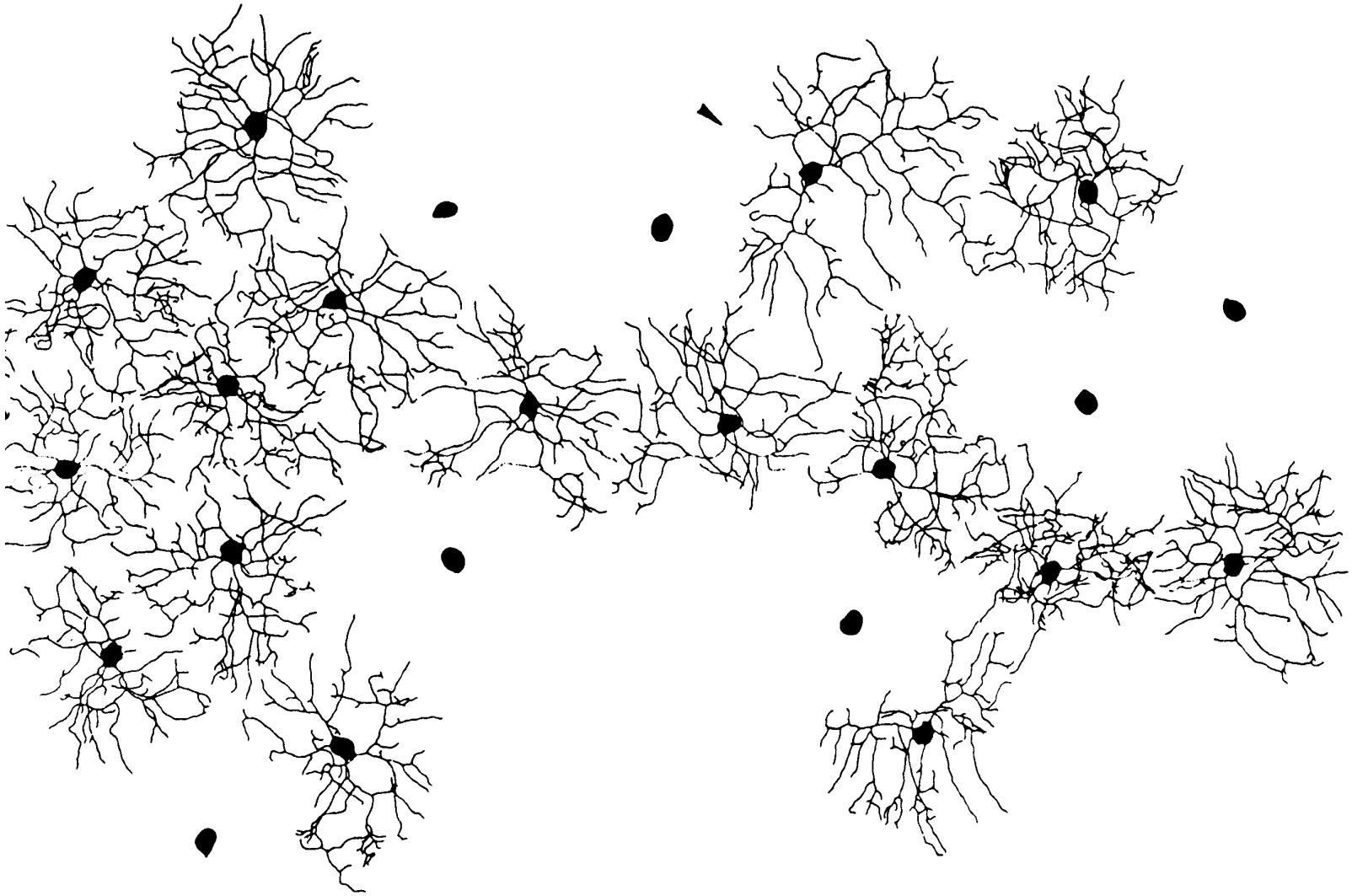

Dacey (1993)

Primate Retinal Ganglion Cell Receptive Field Mosaics

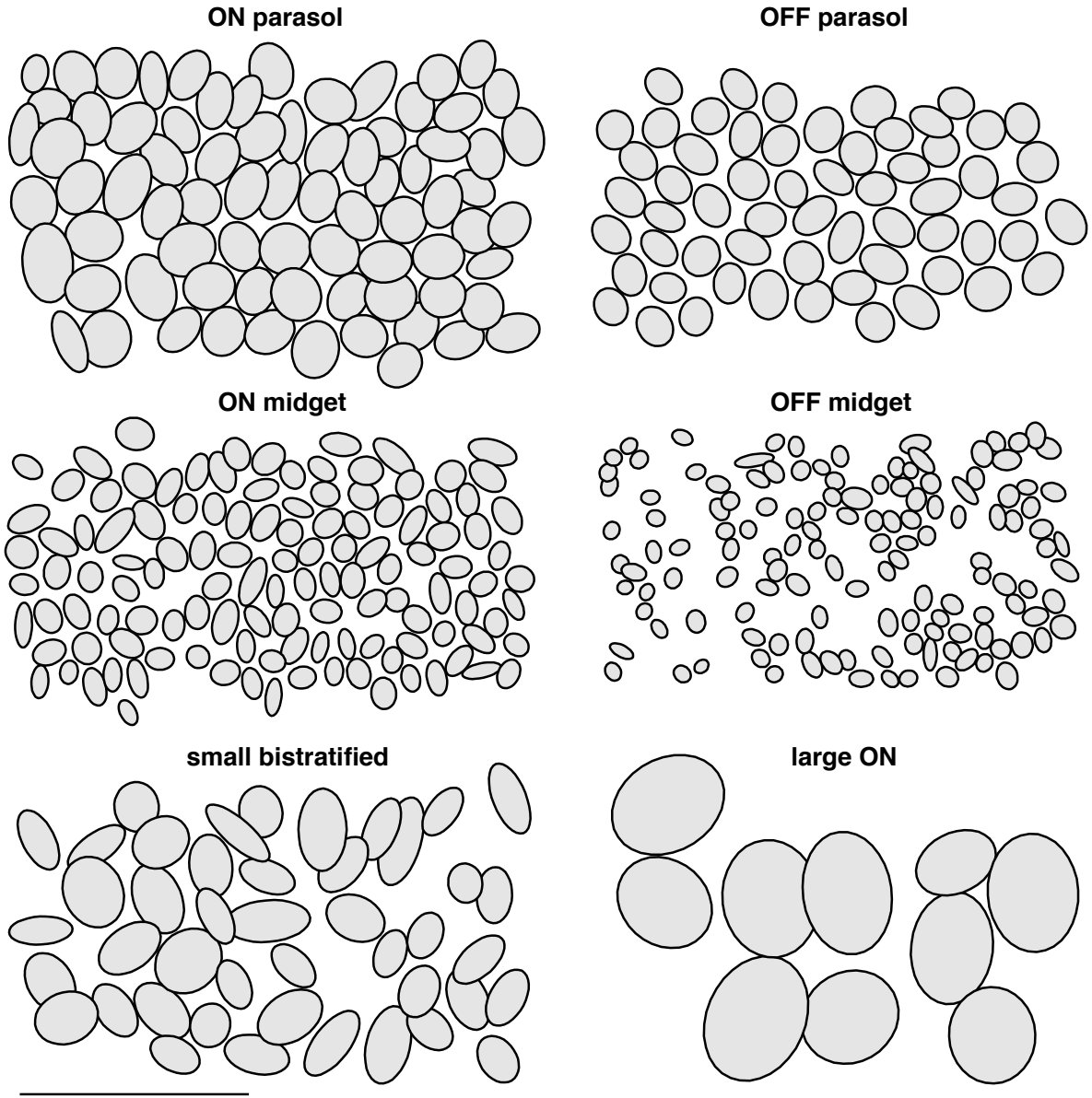

Field & Chichilnisky (2007)

Coordinated Fine Structure of Receptive Fields

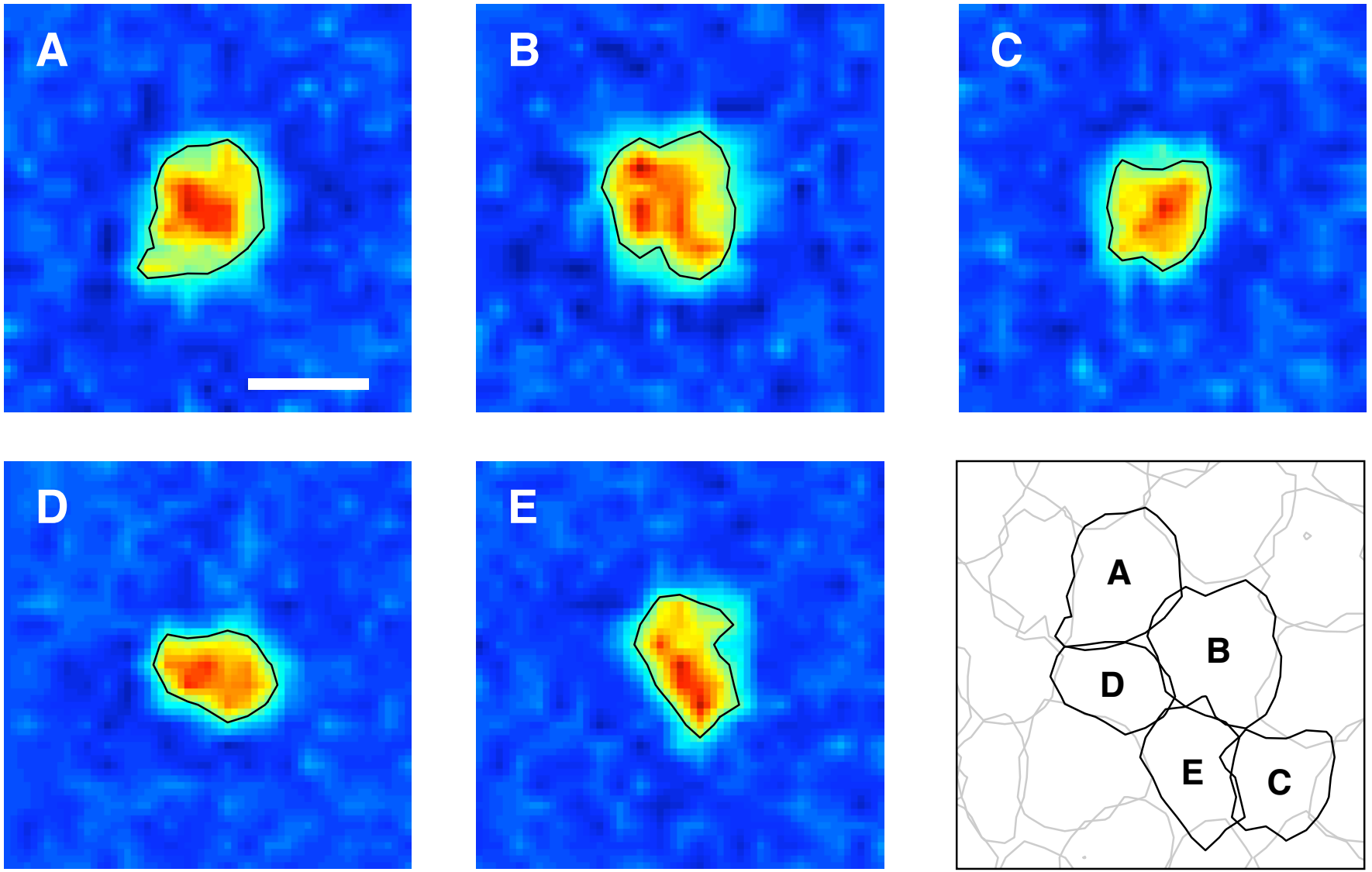

Diversity of ganglion cell morphology in macaque retina (Dacey, 2004)

Monostratified cells are on- or off-center. Bistratified cells are on-off.
The midget and parasol cells (left) are the most common and best-studied types, and project to the parvocellular and magnocellular divisions of the LGN. Other types are "non-M, non-P" and some project to the interlaminar nuclei of the LGN.

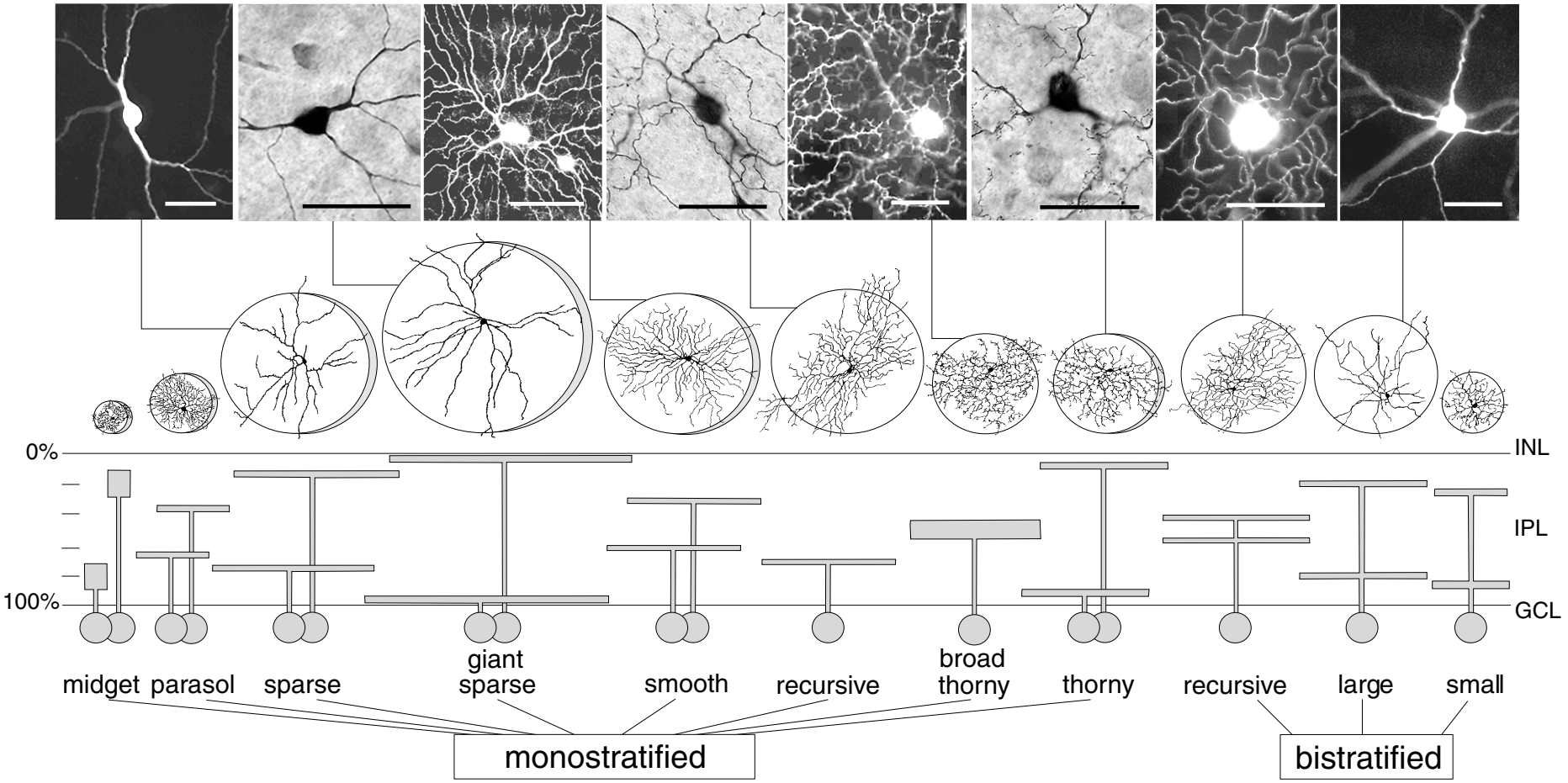

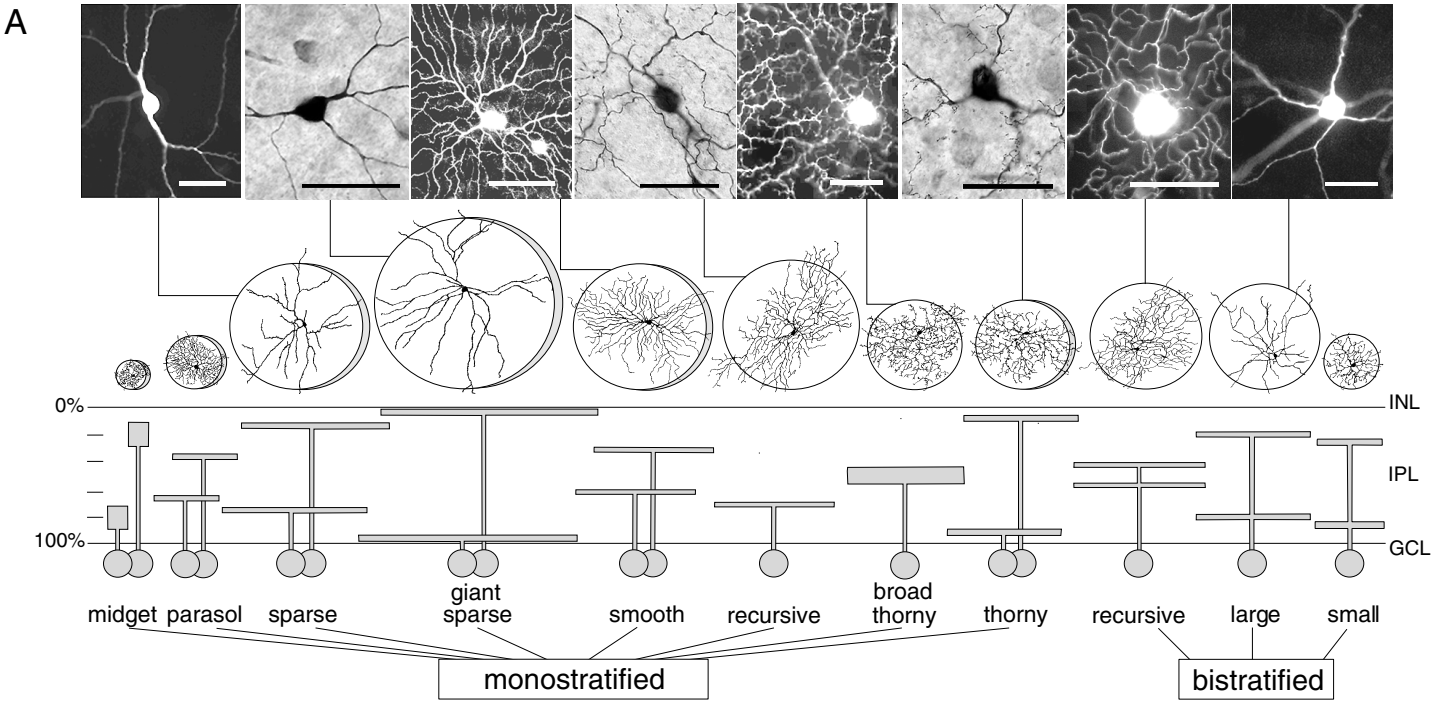
A
0%
100%
INL
IPL
GCL
midget
parasol
sparse
giant sparse
smooth
recursive
broad thorny
thorny
recursive
large
small
monostratified
bistratified

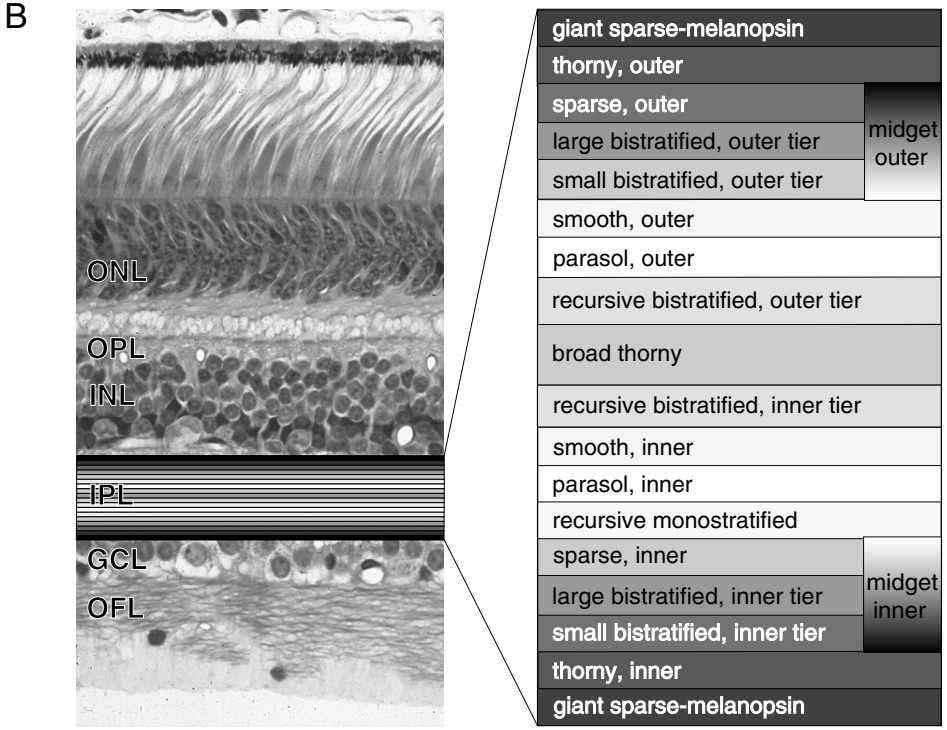
B
ONL
OPL
INL
IPL
GCL
OFL
giant sparse-melanopsin
thorny, outer
sparse, outer
large bistratified, outer tier
small bistratified, outer tier
midget outer
smooth, outer
parasol, outer
recursive bistratified, outer tier
broad thorny
recursive bistratified, inner tier
smooth, inner
parasol, inner
recursive monostratified
sparse, inner
large bistratified, inner tier
small bistratified, inner tier
midget inner
thorny, inner
giant sparse-melanopsin

Dacey, 2004

Cell-type classification and receptive fields at single-cone resolution.

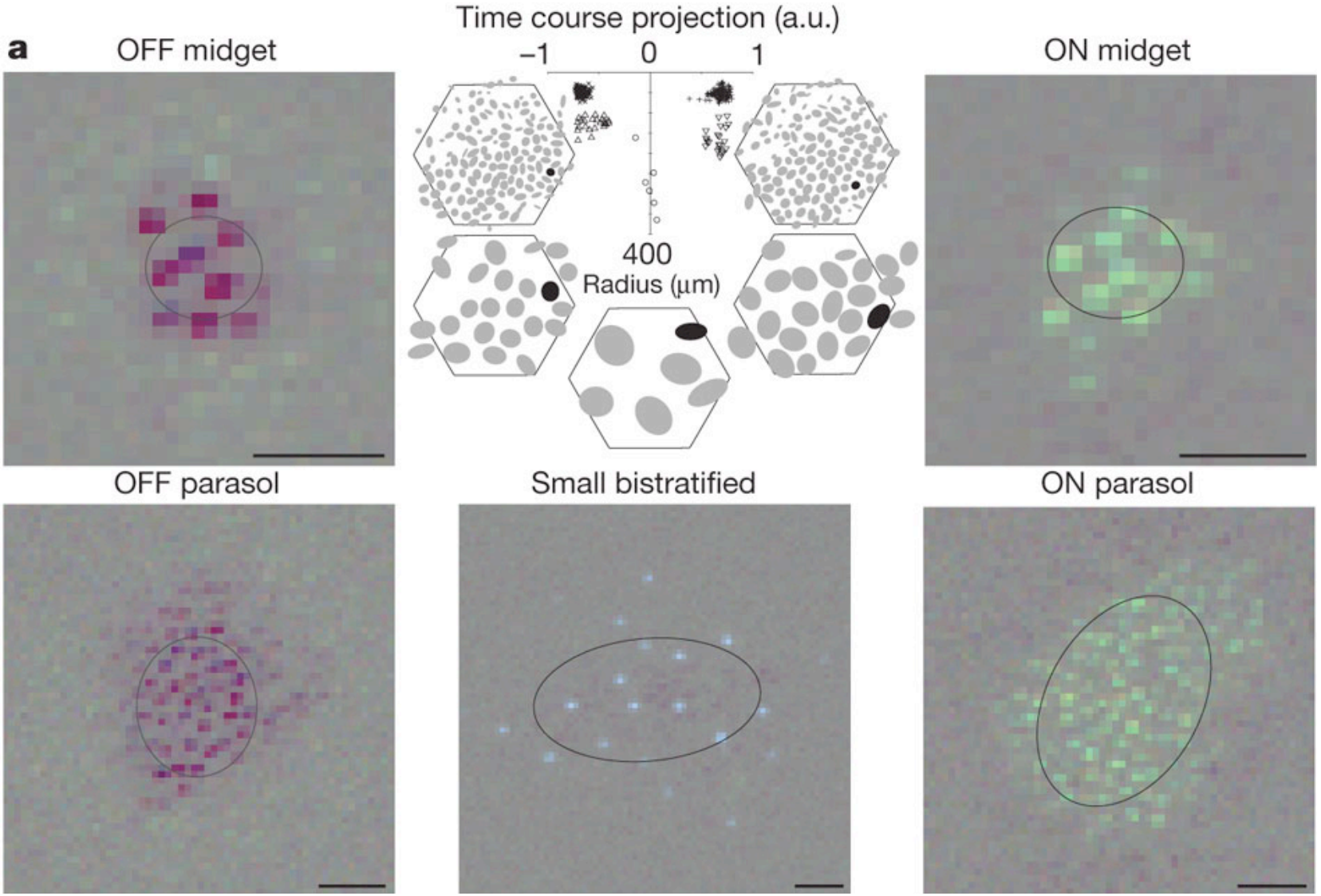

a, Receptive fields of 323 RGCs recorded simultaneously from isolated macaque retina were measured using reverse correlation with white noise stimuli. Centre panel shows receptive-field radius versus first principal component of response time course; clusters reveal distinct cell types. a.u., arbitrary units. Hexagons surrounding centre panel show outline of electrode array and ellipses show Gaussian fits to receptive fields of cells from each cluster. The outer panels show fine-grained spatial receptive-field profiles for highlighted cells. Scale bars, 50 μm

nature
GD Field *et al. Nature* **467**, 673-677 (2010)
doi:10.1038/nature09424

Cone-type identification and inputs to RGCs.

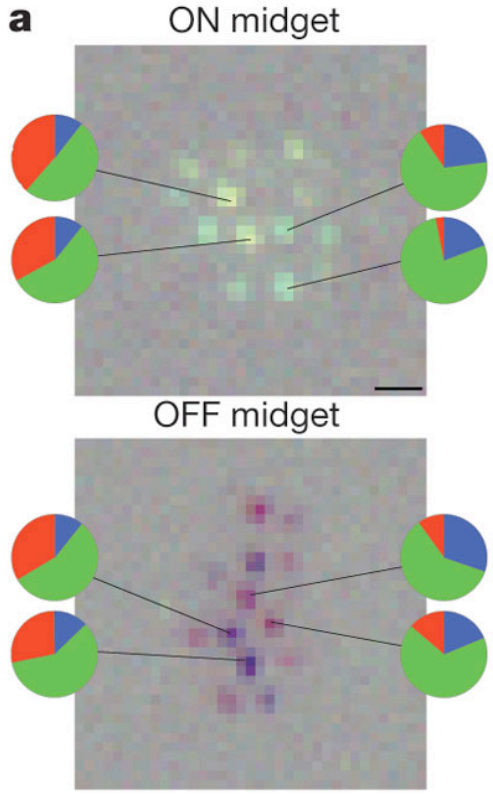

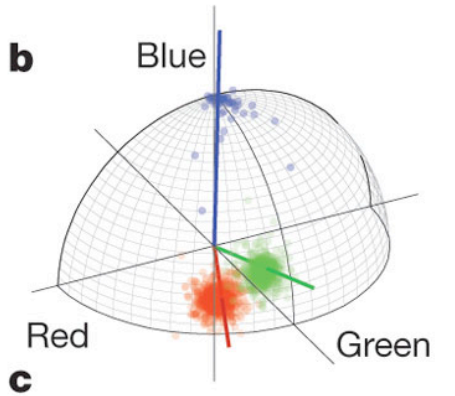

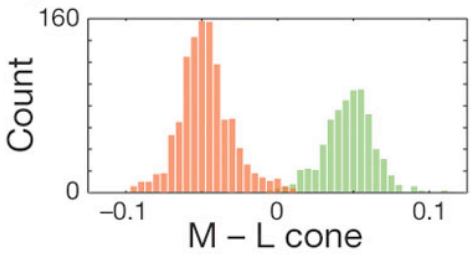

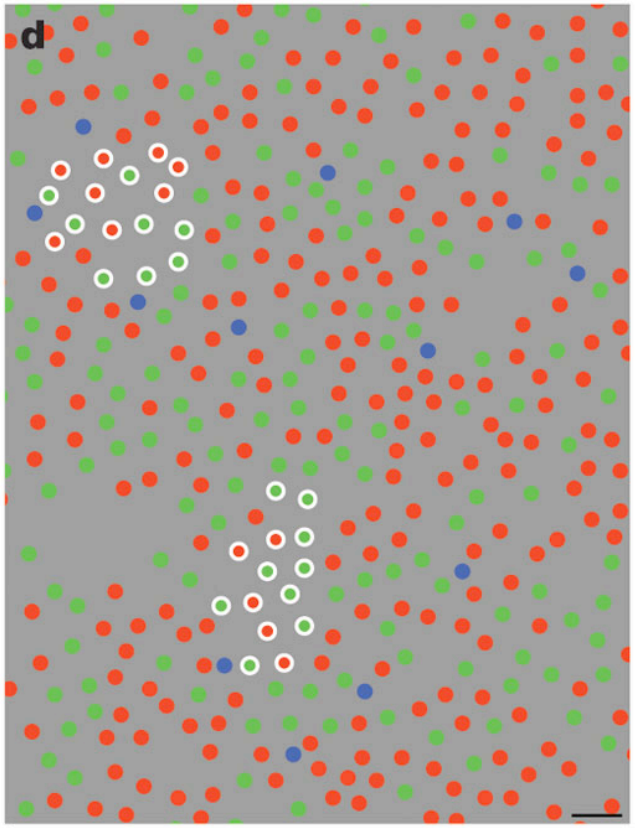

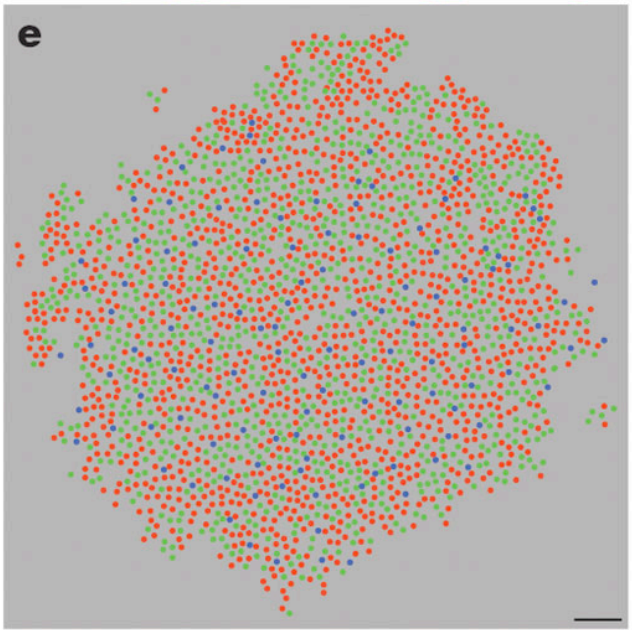

a, The spectral sensitivity of cones providing input to two cells is represented by the relative magnitude of the red, green and blue spike-triggered average values (a.u.) at their locations.

b, For every cone in one recording, these values are shown as points on a sphere. Coloured lines indicate spectral sensitivity of macaque cones. Point colour indicates classification as L (red), M (green), or S (blue).

c, L- and M-cone discriminability quantified by projection along the line joining L- and M-cone loci. Bar colour indicates classification. S cones excluded.

d, Assembled cone mosaic from all RGCs over a region. Cones from **a** are circled.

e, Full mosaic of 2,373 cones from one recording

nature
GD Field *et al. Nature*
467, 673-677 (2010)
doi:10.1038/nature09424

Full functional sampling of cone lattice by four RGC types

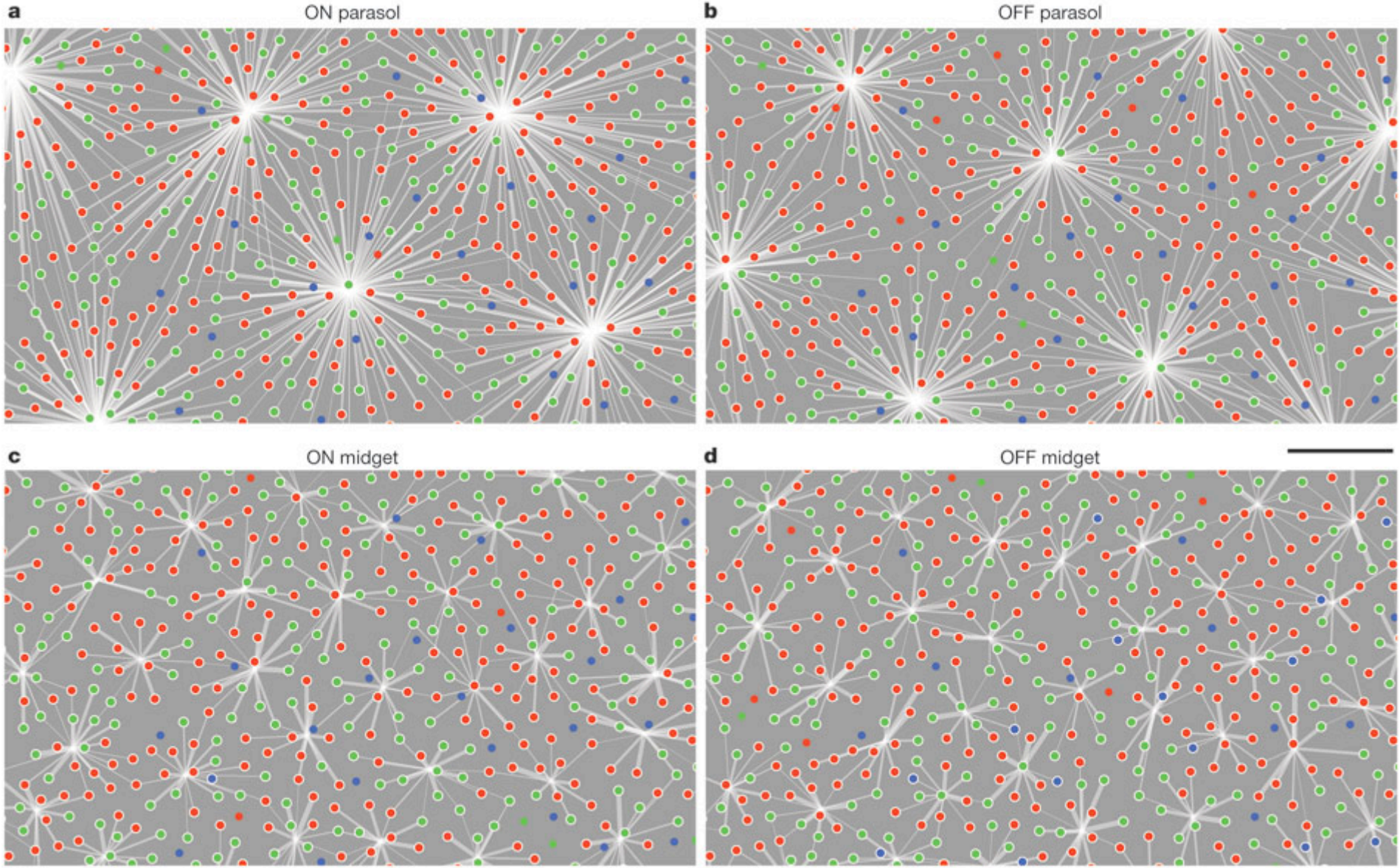

Each panel shows cones identified in a single recording (red, green and blue dots) sampled by receptive-field centres of RGCs of a single type. Cones are identical in all panels. Cones providing input to at least one RGC are highlighted with an annulus. Scale bar, 50 μm.

nature
GD Field *et al. Nature*
467, 673-677 (2010)
doi:10.1038/nature09424